LOW BANDWIDTH ROBUST CONTROLLERS FOR FLIGHT
Grant NCC 2-711

Final Report

June 1991- December 1992

by

Dr. Daniel J. Biezad
Principal Investigator
(805) 756-5126

and

Hwei-Lan Chou
Graduate Student

Aeronautical Engineering Department
Cal Poly State University
San Luis Obispo, CA 93407

presented to

Mr. Glenn Gilyard
NASA Technical Officer
(805) 258-3724

Propulsion and Performance Branch, D-2112
XRP PO 273, NASA Dryden
Edwards, CA. 93523

SYNOPSIS

This is the final report for NASA Grant NCC 2-711. During the final reporting period (June 1992 - December 1992) analyses of the longitudinal and lateral flying qualities were made for propulsive-only flight control (POFC) of a Boeing 720 aircraft model. Performance resulting from compensators developed using Quantitative Feedback Theory (QFT) is documented and analyzed. This report is a first draft of a thesis to be presented by graduate student Hwei-Lan Chou. The final thesis will be presented to NASA when it is completed later this year.

The latest landing metrics related to bandwidth criteria and based on the Neal-Smith approach to flying qualities prediction were used in developing performance criteria for the controllers. The compensator designs were tested on the NASA simulator and exhibited adequate performance for piloted flight. There was no significant impact of Quantitative Feedback Theory on performance of the propulsive-only flight controllers in either the longitudinal or lateral modes of flight. This was attributed to the physical limits of thrust available and the engine rate of response, both of which severely limited the available bandwidth of the closed-loop system.

The following papers were completed in support of this grant:

1. Biezad, D.J. and C.P. Azzano, "Designing Low Bandwidth Propulsive-Only Flight Controllers", AIAA Guidance, Navigation, and Control Conference, Paper #91-2628CP, New Orleans, La., August 12-14, 1991, pp 267-275.

2. Biezad, D.J., "The Propulsive-Only Flight Control Problem," National Aerospace Electronics Conference, Vol 2, pp494-500, Dayton, Ohio, May 20-24, 1991.

3. Chou, H.L. and D. J. Biezad, "Pilot-in-the-Loop Analysis of Propulsive-Only Flight Control Systems," NAECON, Volume 2, pp 482-488, Dayton, Ohio, May 18-22, 1992.

4. Chou, H.L. and D. J. Biezad, "Application of QFT to the Problem of Failed In-Flight Controllers During Approach and Landing," (in preparation)

TABLE OF CONTENTS

List of Tables

List of Figures

Synopsis

Flight control using throttles only to achieve safe landing for a large jet transport airplane, Boeing 720, was investigated. Through throttle manipulations, engine thrust can be used for emergency flight control for multi-engine aircraft. NASA Dryden has studied the use of throttles for emergency flight control and found, in general, manual fly-by-throttle is extremely difficult, with landing almost impossible, but control augmentation makes runway landings feasible.

An augmented control developed in previous simulation study for Boeing 720(B-720) Throttle-Only Flight control(TOFC) has obtained generally good pilot rating, but with light Dutch-roll damping and low control bandwidth that needs to be improved. A control design technique, Quantitative Feedback Theory(QFT), and a linearized B-720 model were employed to analytically study the B-720 TOFC and to optimize the previously developed augmented control.

The fidelity of the linear model was first examined and then modified. Poor open-loop characteristics were observed. The response frequency for pitch control has been increased and the Dutch-roll damping doubled. To improve the control bandwidth substantially proved very difficult. The pitch control designed by QFT showed consistently better results for robustness and for response under no turbulence and turbulence. The roll control by QFT performed better than the roll control built by simulation study when no turbulence was present, but not as well under intermediate turbulence. Applying differential throttle control to engines mounted at different x-y planes from c.g., to produce more instantaneous pitching moment may be a effective way to increase the control bandwidth. Handling qualities of the augmented control for cruise and landing will be evaluated by piloted simulation flight.

Notation

TOFC	Throttle-Only Flight Control
QFT	Quantitative Feedback Theory
C_{mu}	nondimensional velocity-pitch coupling derivative
$C_{\ell\beta}$	nondimensional yaw-roll coupling derivative
q	pitch rate (deg/sec)
γ	flight path angle (deg)
β	angle of sideslip (deg)
φ	bank angle (deg)
θ	pitch angle (deg)
z	thrust (lbs)
ω_i	natural frequency
ζ	damping ratio
δ_{Tc}	stick input(full deflection=1 unit)
K_q	pitch rate feedback gain

K_γ	flight path angle feedback gain
K_β	sideslip angle feedback gain
K_ϕ	bank angle feedback gain
G_{in}^{out}	transfer functons
(a)	short form of (s+a)
[z, w_n]	short form for $s^2 + 2\zeta\omega_n s + \omega_n^2$
D.R.	Dutch-roll
s.p.	short peroid
c.g.	center of gravity

1. Introduction

Through throttle manipulations, engine thrust has been found useful in providing some controllability for multiengine aircraft in emergency situations with severe or complete flight control system failures. NASA has studied the use of throttles for emergency flight control for a range of airplanes[1-6]. Many multiengine airplanes exhibited some degree of useful control capability with the throttles. In general, manually flying an aircraft using throttle-only requires tremendous pilot workload and makes landing extremely difficult to almost impossible. Control augmentation using feedbacks and direct coupling of the throttle command to stick/thumbwheel motion has greatly improved the flying qualities and successful landings could be made.

An augmented control developed in previous studies for B-720 TOFC[1-2], implemented on a high fidelity B-720 flight simulator(Fig.1 &2), had obtained generally good pilot rating. However, its light Dutch-roll damping and low control bandwidth are desired to be improved for better handling qualities. The primary aim of this study is to use an alternative control design technique, Quantitative Feedback Theory(QFT), and a linearized B-720 model to analytically study the B-720 TOFC and to improve the Dutch-roll damping and control bandwidth for better handling qualities.

The QFT technique[18-23] was chosen because of its unique features and of the good insights it provides throughout its design process. It allows designers to specify a desired close loop frequency response with a desired control bandwidth and damping characteristic, and then designs controllers and prefilters to meet the prescribed specifications. The desired performance can't always be achieved within the given control actuation and rate limits; nevertheless, the technique provides good insights to show clearly what has prevented the implementation. The designer can thus have better understanding and make better judgment for the system being investigated.

In this report, the concepts of throttles only flight control is introduced and an augmented throttle-only flight path control for approach and landing for B-720 is built using the QFT technique applied to the linear B-720 model. The fidelity of the B-720 linear model is first examined. The B-720 engine model and the open-loop bare airframe response are then analyzed and discussed. Augmented control design using QFT is

presented in a step by step procedure and Its results are compared with the one from the previous simulation study. Conclusions and recommendations are then made for future studies.

2. Concepts of Throttle-Only Flight Control

The propulsion system of a multi-engine aircraft can be used for heading and flight path control. Differential throttle is applied to control roll through yaw and symmetric throttle to control pitch. Speed control by throttles becomes ineffective when control system fails. Other means may be used to change airplane's speed. Throttles are coupled to stick/thumbwheel for easier and more conventional control handling.

Pitch Control Symmetric throttle induces a speed change which in turn generates a pitching moment change through speed stability effects-C_{mu}, this is the primary source of pitch control. A smaller but immediate pitching moment change is contributed by the offset of thrust vector to the c.g. of the aircraft. Engines mounted at different x-y planes from c.g. can produce additional instantaneous pitching moment by applying differential throttle control. This was proposed initially as a control strategy, but has not been investigated yet.

Yaw-Roll Control Differential thrust generates sideslip, which in turn generates rolling moment changes through wing dihedral and sweep effect-$\mathbf{C}_{\ell\beta}$. Roll is controlled by applying differential throttles to obtain desired bank angle to make turns and heading changes.

Speed Control Retrimming speed by throttles becomes ineffective with primary control surfaces locked due to control systems failure. When control system failure occurs at speed other than landing speed, retrimming to an acceptable landing speed may use other techniques, such as moving c.g. aft, lowering flaps, extending landing gears and variable stabilizer control to reduce speed.

Couple Throttle Command to Stick/Thumbwheel Motion Direct coupling of the throttle command to stick/thumbwheel motion has eased the pilot's handling of control and allowed him to control the airplane in a conventional fashion, i.e. pitch up with stick forward, pitch down with stick aft, and etc.

3. B-720 Linear Model

The B-720 linear model was derived from perturbations of the full non-linear equations of motion about trim and was completely decoupled in longitudinal and lateral dynamics.

The fidelity of the linear model was examined by comparing the open-loop response of the linear model with the nonlinear as shown in Fig. 3 & 4. In Fig. 3, the longitudinal response of the linear model was about 30% less in magnitude than the

nonlinear's, and was, therefore, modified by a correction factor of 1.3. The result after modification is shown in Fig. 5. The linear design used a computer control package "CC" to assist the design.

The lateral response in Fig. 4 showed the linear model would closely follow the nonlinear model as long as the small perturbation assumption was not violated, i.e. the command input should be of small magnitude and short duration.

Fig. 3 & 4 also showed that for the nonlinear model, a flight path angle command would induce little coupling in roll/yaw while a bank angle command induced pronounced pitch coupling. Coupling between longitudinal and lateral modes was completely absent for the linear model.

4. Engines and Bare Airframe System Analysis

4.1 Engines

The spool-up and spool-down engine dynamics for the B-720 engine are shown in Fig. 6a. The empirical transfer function developed is given in short form notation by

$$G_{\delta_{Tc(\%)}}^{Z(lbs)} = \frac{275}{(.55)(5)}$$

The above equation is illustrated in Fig. 6b over low frequency ranges up to 1.0 rad/sec.

4.2 Bare Airframe

It is apparent from the engine bode diagram that severe bandwidth attenuation occurs beyond frequencies of 1 rad/sec. It may not be possible, therefore, to increase the closed-loop bandwidth beyond 1 rad/sec within the range of available thrust.

This can be seen in the pitch rate "q" to thrust "z" transfer function of the bare airframe shown in Fig. 7. The full-order transfer function $G_{\delta_{Tc(\%)}}^{q(deg/sec)}$ shows that 80 db of gain must be added to yield a crossover frequency beyond 1 rad/sec. This corresponds to 10,000 lbs of full thrust from each engine, which would not be practical for approach and landing.

A low order fit to $G_{\delta_{Tc(\%)}}^{q(deg/sec)}$ is also depicted in Fig. 7 and is very accurate near the phugoid frequency. Piloted flight of the unaugmented aircraft was consistently level 3. The main difficulties were the lightly damped phugoid and the low bandwidth throttle control.

The accuracy of the low order fit near the phugoid frequency means that, to a first order approximation, the phugoid frequency and damping are found from:

$$2\zeta\omega_n = -X_u + \frac{M_u(X_\alpha - g)}{M_\alpha}$$

$$\omega_n^2 = \frac{-g(Z_u - \frac{M_u}{M_\alpha}Z_\alpha)}{U_o}$$

and for conventional transport aircraft can be shown to be roughly proportional to M_u.

It should be strongly noted here for the classic case of M_u=0 and for negative values of M_u (Mach tuck) that the aircraft cannot be practically flown with throttle alone unless rotational control in pitch is added. Difficulties will also be encountered as M_α becomes small (aft c.g. location.) Both of these cases require the addition of an effective rotational controller about the pitch axis. This may be achieved using differential inboard and outboard thrust, provided the inboard engines are a different distance from the aircraft xy-plane than the outboard engines. These configuration characteristics determine the innate capability for throttles-only piloted control.

5. QFT Control Design

An overview of QFT design technique is presented in Appendix B.

In the following, a brief procedure of QFT technique is introduced. QFT is a frequency domain control technique that uses a fairly direct and transparent design approach. In order to apply QFT, a system must be modeled as a SISO/MISO unit feedback system. For MIMO systems, a m x m MIMO system can be converted into m - equivalent SISO/MISO system. QFT technique allows designers to specify a desired performance specification and then incorporates the plant uncertainty and system disturbance to form design constraints - performance bounds and a U contour.

After the design constraints are formed, they are displayed on the Nichols Chart together with the plant transfer function. A controller will then be selected to reshape the plant transfer function to satisfy these constraints. After satisfying all the design constraints, if possible, the system is guaranteed robust over the full range of plant uncertainty but may not completely meet the performance specification yet. A prefilter is usually required to reposition the compensated system, shown on a frequency plot, to fully meet the specification.

A QFT computer control package was used to assist the design. the program can apply QFT on minimum-phase plants only, i.e. the plants should have no zeros in the right half s-plane, and only the gain of the desired close-loop performance will be specified and then satisfied. For nonminimun-phase plant, the phase of the desired close-loop performance shall also be specified and satisfied.

The QFT technique for B-720 TOFC design is presented in steps as follows:

5.1 System Modeling

To apply QFT, a system should be in a unit feedback form as shown in Fig. B-1. The B-720 pilot simulation block diagram of flight path and bank angle control are presented below:

Flight Path Angle Control Block Diagram

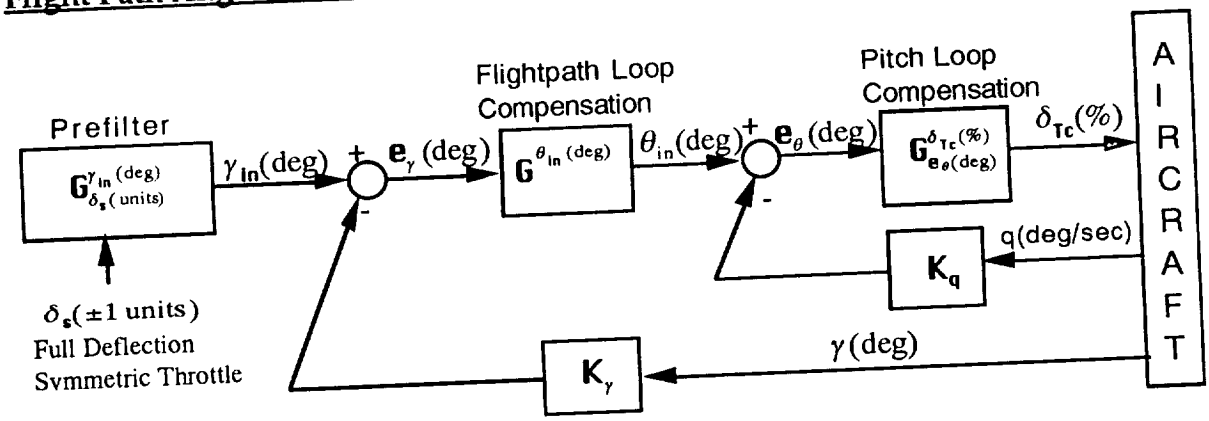

Bank Angle Control Block Diagram

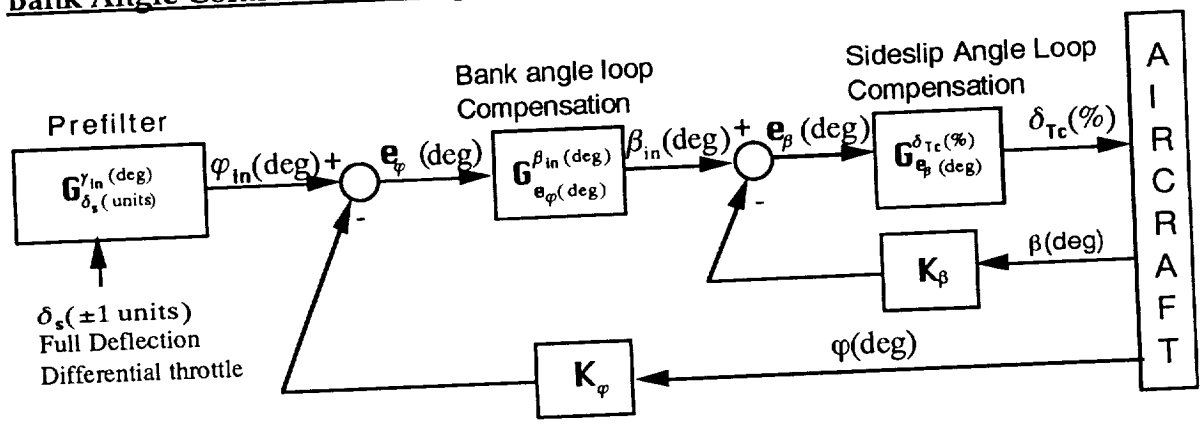

The inner loop was closed first using the same design procedure as will be illustrated in the following. With the inner loop closed, the controls are presented in a unit feedback form as shown below:

Flight Path Angle Control Block Diagram with Inner Loop Closed

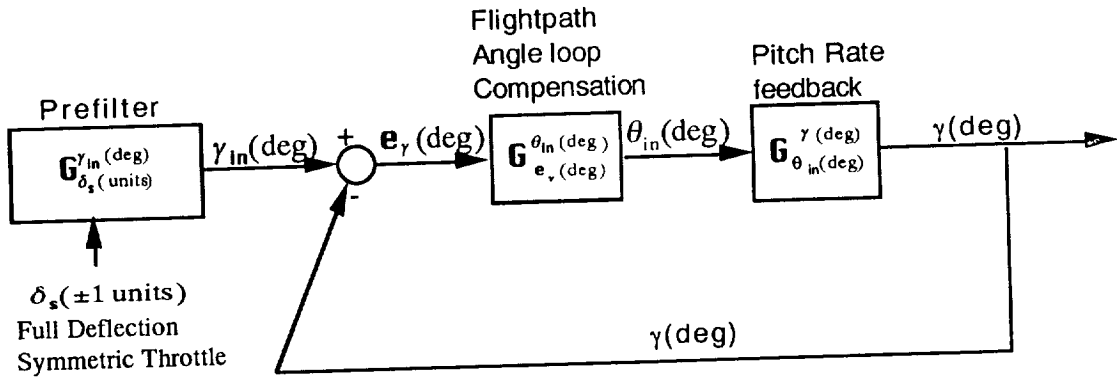

Bank Angle Control Block Diagram with Inner Loop Closed

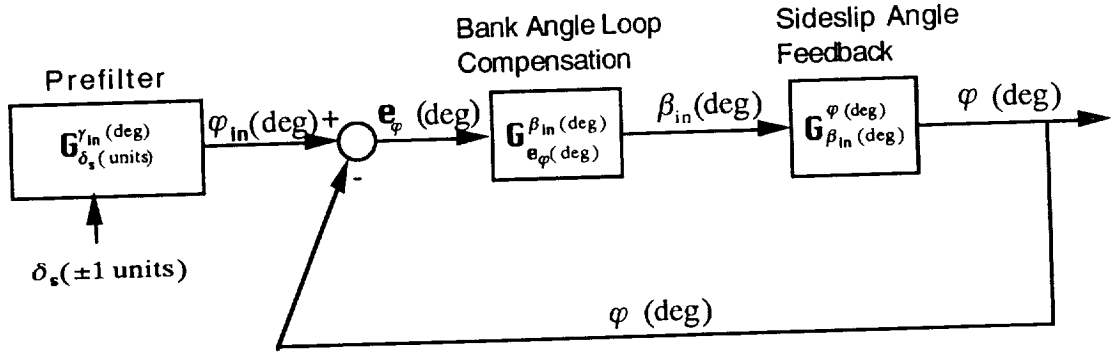

5.2 Performance Specification

QFT allows designers to specify a desired close loop frequency response with an upper bound, B_u, a lower bound, B_L, and a tolerance, δ_R, and also a maximum peak magnitude, M_m(see Fig. B-4). The tolerance, δ_R, is specified to obtain robust performance, and the maximum M_m to obtain a desired system damping.

The upper bound, B_u, is usually described as an underdamped response of a second order system, while the lower bound, B_L, an overdamped response. B_u can be determined by satisfying some or all of the desired performance specifications, {M_p, t_p,t_s,t_r,K_m}, and B_L by satisfying {t_s, t_r, K_m}[23 p.693]. For example, if the desired specifications are: damping ratio z=0.6, rise time t_p=5 sec, and t_s=10 sec, then B_u for the flight path angle and bank angle feedback loops can be modeled as follows:

$\because \varsigma = 0.6$, and $t_p = \frac{\pi}{\omega_n\sqrt{1-\varsigma^2}} = 5$ sec

$\therefore \omega_n = .78$ rad / sec , $M_p = 1 + e^{\frac{-\pi\varsigma}{\sqrt{1-\varsigma^2}}} = 1.09$ and $t_s = \frac{4}{\varsigma\omega_n} = 8.7$ sec $\leq$ 10 sec

since $T_{R_u} = \frac{G_{eq}}{1+G_{eq}}$ and $G_{eq} = \frac{\omega_n}{s(s+2\varsigma\omega_n)}$

therefore, $T_{R_u} = \frac{.61}{s^2+.94s+.61}$

a zero at $s = -5$ is added to T_{R_u} to widen the δ_R at high frequencies

thus $B_u = T_{R_u} = \frac{3.05\,(s+5)}{(s^2+.94s+.61)}$ and $Lm_m = .30$ db

And B_L can be modeled:

$\because t_s = \frac{4}{\varsigma\omega_n} = 8.7$ sec and $\varsigma \geq 1$,

$\therefore \omega_n \leq 0.76$ rad / sec

therefore, $T_{R_L} = \frac{K}{(s+\sigma_1)(s+\sigma_2)} = \frac{.385}{(s+.55)(s+.7)}$

where σ_n should be $\leq \omega_n$,

and t_s of T_{R_L} need to be $\leq$ 10 sec

a pole at $s = -2$ is added to T_{R_L} to widen the δ_R at high frequencies

thus $B_L = T_{R_L} = \frac{0.77}{(s+.55)(s+.7)(s+2)}$

The magnitude of B_u and B_L, and δ_R at each frequency can thus be obtained and are shown in Table 1.

Table 1. Preliminary performance specification

Frequency(rad/sec)	0.1	0.3	0.5	0.7	1.0	2.0	5.0
Bu(dB)	0.0	0.0	0.3	-1.0	-4.0	-15.0	-30.0
BL(dB)	-0.2	-2.0	-4.7	-7.1	-12.4	-24.1	-45.0
δ_R (dB)	0.2	2	5	6.1	8.4	9.1	15.0

The performance specification obtained above is the desired closed-loop response for γ - and φ -loops with no pilot interface. Since these two feedback loops will become the pilot open-loops, additional specifications: a desired control bandwidth (BW) of 2 rad / sec for landing tasks for transport aircraft(see ref. 17) and a k/s gain slope

near crossover frequency, need to be added in order to obtain good pilot handling qualities. The QFT technique describes here applies only to minimum phase systems. Since in a minimum phase system the magnitude of the frequency response completely specifies the transfer function, hence the BW_{gain}, the bandwidth determined by the frequency at -3 db, can solely determine the system bandwidth. The B_u and B_L acquired is, therefore, needed to be raised to meet the additional specifications. The performance specification is finalized as shown in Table 2 and Fig. 8.

Table 2. Final performance specification

Frequency(rad/sec)	0.1	0.3	0.5	0.7	1.0	2.0	5.0
B_{u}(dB)	17.0	17.0	17.3	16.0	13.0	2.0	-13.0
B_{L}(dB)	16.8	15.0	12.3	9.9	4.6	-7.1	-23.0
δ_R (dB)	0.2	2	5	6.1	8.4	9.1	15.0

5.3 Design constraints

The performance bounds constraint is a curve on Nichols Chart that constructed by mapping the template in s-plane, formed by plant uncertainties, onto the Nichols Chart to match the performance tolerance, δ_R(see Fig. B-2 & 3). Therefore, satisfying this constraint guarantees the variation of the system response due to plant uncertainties will be no greater than δ_R. When the template of plant uncertainty in s -plane is mapped onto Nichols chart(jω-plane), the template transforms into different shape for each different frequency. Thus, there is a performance bound for each frequency.

The U contour is a M-circle on the Nichols Chart that has the magnitude of M_m, with part of the circle stretched for uncertainty at high frequencies. By having the system not penetrating the U contour, the system's damping will be guaranteed no less than the damping correlating to M_m .

5.4 Airplane Parameter Uncertainty

Four configurations were given to study the approach and landing of B-720 throttle-only flight control. The flight condition of these configurations are summarized in Table 3. Configuration 1 was used as the nominal confiuration for control design.

Config. Number	Weight (lbs)	Altitude (Ft MSL)	Airspeed (Knots)	Flaps (%)	Gear up/down
1	140,000	4,000	160	0	up
2	140,000	4,000	145	30	up
3	160,000	4,000	175	0	up
4	140,000	4,000	155	30	up

Table 3. Flight condition of the four configurations given for B-720 TOFC approach and study

A robust controller is highly desirable for systems undergoing constant changes such as aircraft. QFT incorporates the plant parameter variation(uncertainty) into design by converting them into design constraints and then builds controllers to satisfy the constraints. An example of a plant with parameter variations is illustrated below:

Example

For a plant transfer function

$$G(s) = \frac{Ka}{(s+a)}, \quad \text{where the parameter variations are: } 1 < k < 10 \text{ and } 1 < a < 10$$

then,

$$G(s)\ \text{min.} = \frac{1}{s+1} \quad \text{and} \quad G(s)\ \text{max.} = \frac{100}{s+100}$$

For inner-loop transfer functions $G^{\gamma}_{\theta_{in}}$ and $G^{\phi}_{\beta_{in}}$, the parameter variation given by the four configurations can be expressed in the same manner :

For longitudinal flight path angle control:

The $G^{\gamma(deg)}_{\theta_{in}(deg)}$ of the nominal configuration(config. 1) is:

$$G^{\gamma(deg)}_{\theta_{in}(deg)}\ \text{config. 1} = \frac{.01(.203)[.37,\ 3.01]}{(.562)[.624,\ .111][.441,\ 1.57](5.25)}$$

and the min. and max. $G^{\gamma(deg)}_{\theta_{in}(deg)}$ are:

$$G^{\gamma(deg)}_{\theta_{in}(deg)}\ \text{min.} = \frac{.0053\ (.162)[.35\ ,\ 3.01]}{(.40)[.42\ ,\ 1.48][.66\ ,\ .01](5.19)}$$

$$G^{\gamma(deg)}_{\theta_{in}(deg)}\ \text{max.} = \frac{.01\ \ (.28)[.46,\ 3.43]}{(.58)[.45\ ,\ 1.57][.92\ ,\ .14](5.24)}$$

For lateral bank angle control:

The $G^{\phi(deg)}_{\beta_{in}(deg)}$ of the nominal configuration(config. 1) is:

$$G^{\phi(deg)}_{\beta_{in}(deg)}\ \text{nomunal} = \frac{.09\,[.47\ ,\ 3.65]}{(.98)\,[.81\ ,\ .15]\,[.26\ ,\ 1.07]\,(5.02)}$$

and the min. and max. of $G^{\phi(deg)}_{\beta_{in}(deg)}$ are:

$$G^{\phi(deg)}_{\beta_{in}(deg)}\ \text{min.} = \frac{.06\,[.45\ ,\ 3.65]}{(.98)\,[.60\ ,\ .15]\,[.24\ ,\ .93]\,(5.01)}$$

$$G^{\phi(deg)}_{\beta_{in}(deg)}\ \text{max.} = \frac{.09\,[.61\ ,\ 4.33]}{(1.03)\,[1.0\ ,\ .20]\,[.29\ ,\ 1.09]\,(5.02)}$$

The minimum and maximum values of transfer functions, $G^{\gamma}_{\theta_{in}}$ and $G^{\phi}_{\beta_{in}}$, are given to form the uncertainty template which will then be used to determine the performance bound constraints as explained in section 5.3. The QFT control package allows the designer to input plant parameter variations by entering the transfer function's maximum and minimum - gain, first order poles and zeros, and second order poles and zeros. However, due to the software's limitation of handling the quantity of uncertainties, some uncertainties have to be averaged instead of a maximum and a minimum. There are tradeoffs between plant parameter variations and performances. The wider spread of the parameter variation, the more restricted the constraints; consequently more compensation is required. Therefore, the performance specification may need to be relaxed when there is not enough control power to provide all the compensation that's required.

5.5 Controller design

Poles/zeros/gain compensation may be required to reshape the inner loop transfer functions, $G^{\gamma}_{\theta_{in}}$ and $G^{\phi}_{\beta_{in}}$ (see control block diagram in sect. 5.1), to satisfy the performance bounds and the U contour constraints. An added gain will raise the transfer function curve, a zero will bend the curve to the right, and a pole will bend the curve to the left. The poles/zeros/gain that selected to achieve the reshaping forms the controller, G_c. $G^{\gamma}_{\theta_{in}}$ and $G^{\phi}_{\beta_{in}}$ after reshaping, become, respectively, $L^{\gamma}_{e\gamma}$ and $L^{\phi}_{e\phi}$, these are the open-loop transfer functions of the flight path angle and bank angle feedback loops (note that $L^{\gamma}_{e\gamma} = G^{\theta_{in}}_{e\gamma} * G^{\gamma}_{\theta_{in}}$ and $L^{\phi}_{e\phi} = G^{\beta_{in}}_{e\phi} * G^{\phi}_{\beta_{in}}$, ref. to block diagrams in section 5.1.) $L^{\gamma}_{e\gamma}$ and $L^{\phi}_{e\phi}$ should be kept on and above the $B_o(jw_i)$, for each frequency, w_i on $L^{\gamma}_{e\gamma}$ and $L^{\phi}_{e\phi}$. This is to assure robust performance. $L^{\gamma}_{e\gamma}$ and $L^{\phi}_{e\phi}$ should also not to penetrate the U contour in order to obtain a desired damping characteristic.

For Longitudinal Flight Path Angle Control: Transfer function $G^{\gamma}_{\theta_{in}}$ and its performance bounds, $B_o(jw_i)$, and U contour are displayed on a Nichols Chart in Fig. 9.

Notice in Fig. 9, all the frequencies on $\mathbf{G}^{\gamma}_{\theta_{in}}$ are below their corresponding $B_o(jw_i)$. Therefore, reshaping is required. Since pure gain compensation is always preferred if possible, hence, $\mathbf{G}^{\gamma}_{\theta_{in}}$ was first raised by increasing the gain of $G_c(= \mathbf{G}^{\theta_{in}}_{\gamma}$ here) to 16, until it touched the U contour as shown in Fig. 10. Poles/zeros compensation was then added to further reshape the $\mathbf{G}^{\gamma}_{\theta_{in}}$ to avoid the U contour while satisfying all the $B_o(jw_i)$. However, no poles/zeros compensation was found that would do so. A zero at .1 rad/sec was first added, which pulled the whole $\mathbf{G}^{\gamma}_{\theta_{in}}$ curve to the right of the U contour, however, once a pole is added, no pole at any location would prevent the $\mathbf{G}^{\gamma}_{\theta_{in}}$ curve from penetrating the U contour, which is least desired. Since compensator with only one zero is phisically unimplementable. Therefore, the compensator, G_c, for the flight path angle feedback loop, $\mathbf{G}^{\theta_{in}}_{e_\gamma}$, is ,a pure gain of 16 and only the U contour constraint was satisfied in order to obtain a desired system damping; the performance bounds, hence the system robustness was left unsatisfied. The frequency response of the close-loop transfer function, $\mathbf{T}^{\gamma}_{\gamma_{in}}$, where $\mathbf{T}^{\gamma}_{\gamma_{in}} = \mathbf{L}^{\gamma}_{e_\gamma} / (1 + \mathbf{L}^{\gamma}_{e_\gamma}) = (\mathbf{G}^{\theta_{in}}_{e_\gamma} * \mathbf{G}^{\gamma}_{\theta_{in}}) / (1 + \mathbf{G}^{\theta_{in}}_{e_\gamma} * \mathbf{G}^{\gamma}_{\theta_{in}})$, is shown in Fig. 11. It can be seen in Fig. 11 that δ_T, the spread between T_{max} and T_{min}, had exceeded the δ_R over the frequency range .1 to .7 rad/sec as a result of leaving $\mathbf{L}^{\gamma}_{e_\gamma}$ not satisfying the performance bounds over that frequency range. To have any frequency, ω_i, on $\mathbf{L}^{\gamma}_{e_\gamma}$ higher than its corresponding $B_o(jw_i)$ will result in $\delta_T(j\omega) \le \delta_R(j\omega)$, while lower than $B_o(jw_i)$ result in $\delta_T(j\omega) \ge \delta_R(j\omega)$. It can also be seen in Fig. 10 that further modification is required to fully meet the prescribed specification. The frequency plot of the close-loop response after adding a prefilter is shown in Fig. 12.

For Lateral Bank Angle Control: Transfer function $\mathbf{G}^{\phi}_{\beta_{in}}$ and its performance bounds, $B_o(jw_i)$, and U contour are displayed on a Nichols Chart in Fig. 13. Notice that $\mathbf{G}^{\phi}_{\beta_{in}}$ is not only below all the $B_o(jw_i)$ but also penetrate the U contour. Therefore, more than just a pure gain is required to reshape $\mathbf{G}^{\phi}_{\beta_{in}}$. A controller, $\mathbf{G}^{\beta_{in}}_{e_\phi}$=(s+.15)/(s+1.5), was added to $\mathbf{G}^{\phi}_{\beta_{in}}$ to reshape it and had avoided it from penetrating the U contour but not successful in satisfying all the $B_o(jw_i)$. After reshaping, $\mathbf{L}^{\phi}_{e_\phi}$ is shown on a Nichols Chart in Fig. 14 and the frequency plot of the close-loop transfer function, $\mathbf{T}^{\phi}_{\phi_{in}}$, where $\mathbf{T}^{\phi}_{\phi_{in}} = \mathbf{L}^{\phi}_{e_\phi} / (1 + \mathbf{L}^{\phi}_{e_\phi}) = (\mathbf{G}^{\beta_{in}}_{e_\phi} * \mathbf{G}^{\phi}_{\beta_{in}}) / (\mathbf{G}^{\beta_{in}}_{e_\phi} * \mathbf{G}^{\phi}_{\beta_{in}})$, is shown in Fig. 15. Again, prefilter is required to further meet the prescribed specification.

5.6 Prefilter Design

Gain/poles/zeros compensation may also be used for prefilter to reshape the close-loop frequency response, $\mathbf{T}^{\gamma}_{\gamma_{in}}$ and $\mathbf{T}^{\phi}_{\phi_{in}}$. It can be seen in Fig. 11, $\mathbf{T}^{\gamma}_{\gamma_{in}}$

needs both gain and lead compensation to raise the whole $T^{\gamma}_{\gamma_{in}}$ curve and to hunch up the curve at high frequencies to fully meet the specification. However, only a maximum gain of 6 is allowed before the control saturation would occur. Lead compensator was tried, it had hunch up the curve, however, it also reduced the gain available to raise the whole curve. Overall, a prefilter of a pure gain of 6 proved most effective in increasing the bandwidth and to meet the prescribed specification. $T^{\gamma}_{\gamma_{in}}$ after adding the prefilter is shown in Fig. 12.

Fig. 15 shows the close-loop frequency response of $T^{\phi}_{\phi_{in}}$ after reshaping but with no prefilter applied yet. Sufficient gain is available here. A lead compensator of (S+1)/(S+2) is added to haunch up the severely deteriorated curve at frequency over 1 rad/sec, and a lag compensator of (S+.25)/(S+.15) is added to steeper the gain curve at low frequencies as to provide a smoother k/s curve for good pilot handling qualities. The close-loop response after adding the prefilter is shown in Fig. 16 and the prefilter selected is 15(S+.25)(S+1)/((S+.15)(S+2)).

6. Results and Discussion

The objective of this study is to improve the B-720 augmented throttle only control, thus the primary task is to increase the low bandwidth and the light Dutch-roll damping. The control bandwidth of the TOFL depends primarily on the engine response to throttle command and on the propulsion-induced low-frequency speed and dihedral stability effects, which are configuration-dependent, thus not subjected to easy changes. Using different control strategy, i.e. different feedbacks, compensations, and/or different control theories may change the response.

For bank angle control, β feedback was found most effective in increasing Dutch-roll damping, the higher the β feedback gain the higher the Dutch-roll damping. Bank angle feedback is crucial to lateral phugoid damping, and yaw rate feedback helps Dutch-roll damping very little while hurting the lateral phugoid damping. Therefore, β- and φ- feedback were chosen for bank angle control. The architecture of the feedback controls are presented in section 5.1. Table 4 lists the comparison of the natural frequency(ω_n) and damping ratio(ζ) of the dynamic modes of the bare airframe, and of the augmented control built by the simulation study and by QFT.

Longitudinal modes	density	phugoid	s.p.	engines
Bare a/f	: (1.4e-6)	[.04,.13]	[.65, 1.4]	(.55) (5.2)
Simulation augmented control	: (4.7e-6)	[.52, .24}	[.52, 1.5]	(.4) (5.2)
QFT augmented control	: (3.4e-6)	[.62, .32]	[.46, 1.6]	(.3) (5.2)

Lateral modes		spiral	engine	D.R.	roll	engine
Bare a/p	:	(1.1e-4)	(.55)	[.12,.99]	(1)	(5)
Simulation augmented control	:	[.73, .35]		[.15, .99]	(1)	(5)
QFT augmented control	:	(.39)	(.45)	[.29, 1.0]	(1.5)	(5)

Table 4 Natural frequency and damping ratio of the dynamic modes of the bare airframe and of the augmented control by simulation atudy and by QFT

For longitudinal control, pure gain compensation was used. Since the short period mode has frequency around 1.5 rad/sec, which is beyond the frequency that throttles can control, therefore, short period damping was traded for phugoid damping and frequency. The short period damping decreased from .52 to .46 rad/sec while the phugoid damping and frequency increased from .52 to .62 and from .24 rad/sec to .32 rad/sec, respectively. This increase of response frequency can also be depicted from the flight path angle response in Fig. 17.

For lateral control, pole/zero compensation was used. The Dutch-roll damping was almost doubled, from .15 to .29. The previously build lateral phugoid mode, [.73, .35], which combines the spiral and the slow engine mode, was replaced by two real root modes, (.39) and (.45), both with higher frequency.

All plots from Fig. 17 to 22 were obtained from simulation runs at approach and landing conditions with major control surfaces(ailerons, elevator sand rudders) locked except the electrical, the mechanical systems and the landing gear remained operative.

The response of the augmented controls built by the simulation study and by QFT were compared in Fig. 17 and Fig. 18. The Dutch-roll oscillation was removed after the damping was increased by QFT(see Fig. 18), while the response frequency increased a little, from 0.35 rad/sec to .39 rad/sec. In both figures, the control magnitude and rate has been increased but remained reasonable.

Turbulence Response The response of the flight path control under intermediate turbulence is presented in Fig. 19. Because of the gust randomness, more than one simulation run was made to examine the tracking integrity under turbulence. The presently build control showed consistently better results.

In Fig. 20, the bank angle tracking of the QFT augmented control performed not very well under intermediate turbulence. Each gust caused too much tracking deviation. It was thought that the not well-behaved tracking is because of the larger K_β gain being used, the K_β was increased from 1 to 4 as can be seen from the list of the compensation built by the simulation study and by QFT:

For longitudinal flight path angle augmented control:

Simulation study compensation:

$$PF = 10\,,\quad G_{e_\gamma}^{\theta_{in}} = 1\,,\quad G_{e_\theta}^{\delta_{Tc}} = 10$$

$$K_\gamma = 1\,,\quad K_q = 4$$

QFT compensation:

$$PF = 6\,,\quad G_{e_\gamma}^{\theta_{in}} = 16\,,\quad G_{e_\theta}^{\delta_{Tc}} = 1$$

$$K_\gamma = 1\,,\quad K_q = 60$$

For lateral bank angle augmented control:

Simulation study compensation:

$$PF = 40\,,\quad G_{e_\beta}^{\beta_{in}} = 1\,,\quad G_{e_\phi}^{\phi_{in}} = 1\,,\quad G_{e_p}^{\delta_{Tc}} = 1$$

$$K_\beta = 1\,,\quad K_\phi = .5\,,\quad K_p = .5$$

QFT compensation:

$$PF = 2.5(S+.25)/(S+1.25)\,,\quad G_{e_\phi}^{\beta_{in}} = 1\,,\quad G_{e_\beta}^{\delta_{Tc}} = 1\,,$$

$$K_\phi = (S+.15)/(S+1.5)\,,\quad K_\beta = 4\,,$$

This larger K_β multiplies the sideslip from gust plus the sideslip output from the airplane four time larger before it was feedback to the airplane. This has dramatic effect on the bank angle output due to the fact that 0.2 degree of sideslip angle would induced approximately 10 degrees of bank angle owing to the large C_{lb} of B-720. Since for B-720 TOFC, b feedback is the only parameter that can effectively increase Dutch-roll damping, a compromise seems necessary between lateral phugoid tracking and Dutch-roll damping.

However, during investigation of resolving the above mentioned bank angle tracking problem, it was found that the β being feedback in the simulation was the β at the c.g. instead of the β at the nose boom. The nose boom β is actually measured and feedback in a real airplane. The nose boom β was then modeled into the B-720 simulator, which improved the bank angle tracking under turbulence. The β at nose boom has two extra terms than the c.g. β, one-a function of roll rate, the other-a function of yaw rate. It was thought that the extra yaw rate term might have stabilized the bank angle tracking (the roll rate term was too small and thus being neglected.) This result seems contradictory to the preliminary investigation, which found yaw rate feedback does not help either Dutch-roll or lateral phugoid mode. Adding yaw rate feedback to bank angle control will be investigated after this preliminary report.

Fig. 21 & 22 show the system response to configuration variations, for flight path control and for bank angle control, respectively. The robustness of the flight path control has been improved by QFT as shown in Fig. 21. Fig. 22 shows the Dutch-roll oscillation in simulation compensation was taken out by QFT compensation, however, the tracking became worse. After this preliminary report, using yaw rate feedback or

using other types of compensation will be investigated to attempt to improve the bank angle tracking problem.

7. Conclusions and Recommendations

Studies by NASA Dryden has shown that throttles can be used for emergency flight control, although manual fly-by-throttle is extremely difficult with landing almost impossible, but with control augmentation runway landing is feasible.

Flight path control by throttles only to achieve safe landing for a transport airplane, Boeing 720, was investigate. Augmented throttles only flight path control build in Previous simulation study has made successful simulation landing, however, has the problem of light Dutch-roll damping and low control bandwidth. The augmented control built by linear analysis using QFT technique has improved the bandwidth and the Dutch-roll damping.

For pitch control, the control bandwidth , tracking and control robustness has all been improve by QFT. For bank angle control, QFT has improved the Dutch-roll oscillation problem and performs well under no turbulence. However, the lateral phugoid tracking under intermediate turbulence does not performed as well. It seems adequate compromise is required between Dutch-roll and lateral phugoid mode. Further investigation will be made on bank angle tracking for bank angle control under turbulence. The bare airframe analysis shows to improve the bandwidth substantially would be difficult due to the engine performances and the low frequency stability effect that provides pitch and roll control. A strategy as proposed initially in this study, to apply differential throttle control to the high and low mounted engines to produce more instantaneous pitching moment may be an effective way to improve response frequency

Acknowledgment

Special thanks to Dr. Dan Biezad for his encouragement, support and guidance. Thanks also goes to Mr. Glen Gilyard and Mr. Bill Burcham for their technical support and guidance, and for granting me the opportunity to gain invaluable experience out of this research.

Figure 1. Boeing-720

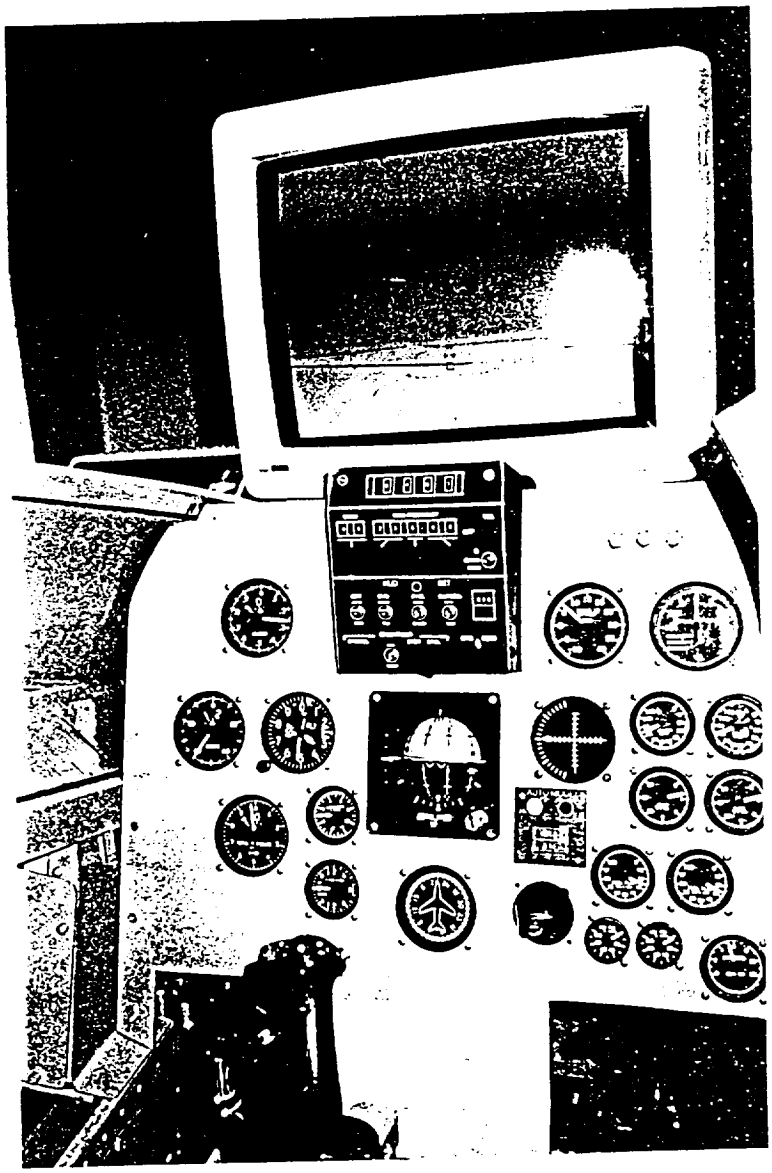

Figure 2. Boeing-720 simulation cockpit

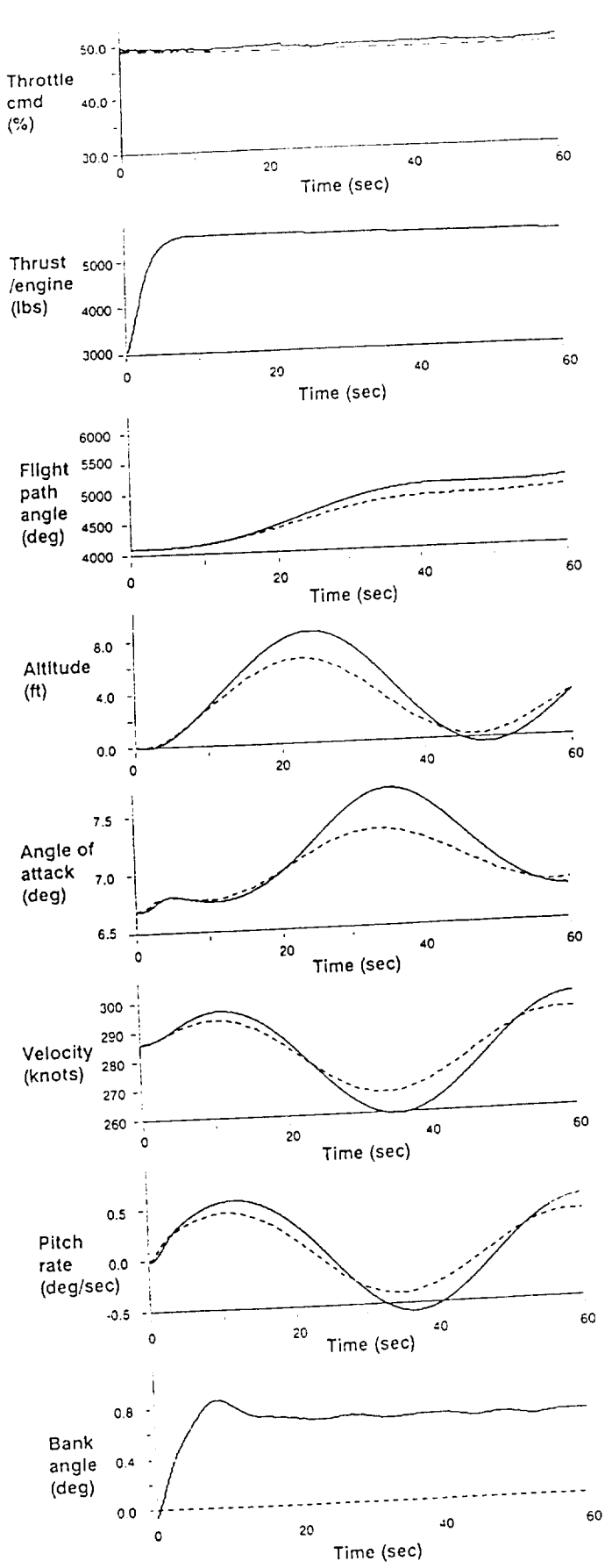

Figure 3. Comparison of the longitudinal open-loop response of the B-720 linear and nonlinear model, 20% step throttle cmd, nominal configuration

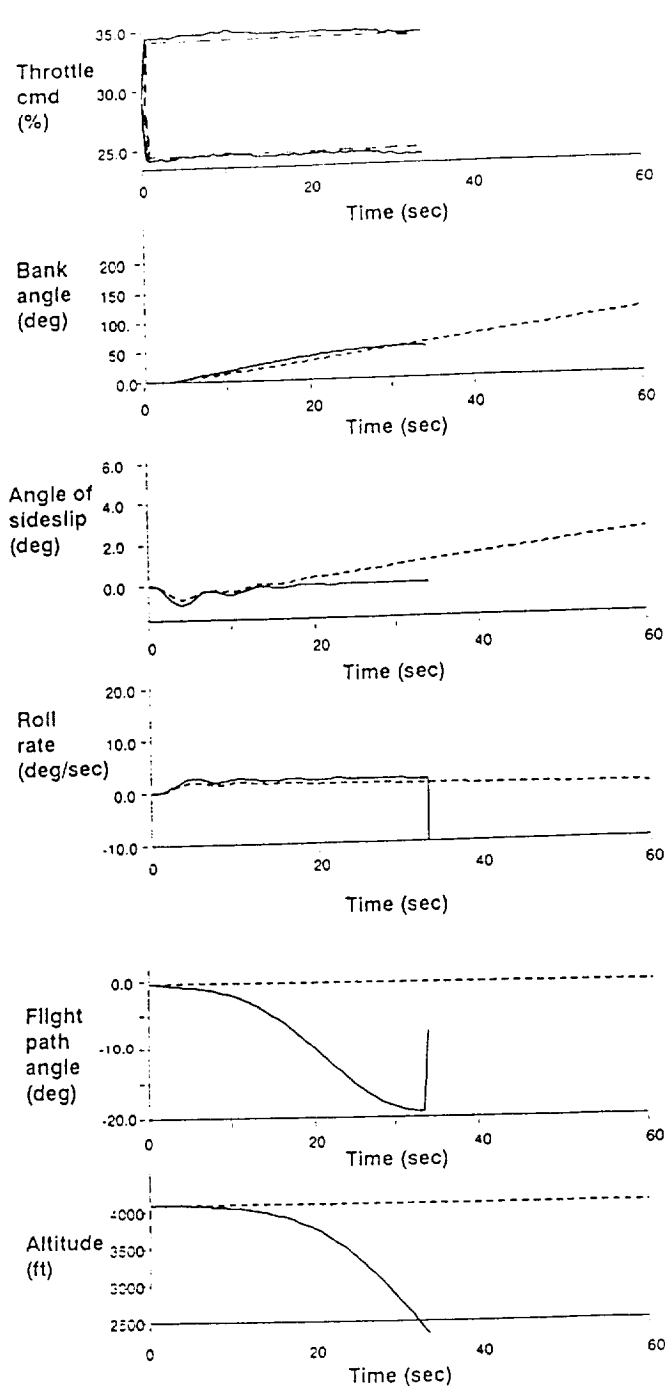

Figure 4. Comparison of the lateral open-loop response of the B-720 linear and nonlinear model, 5% differential throttle, nominal configuration

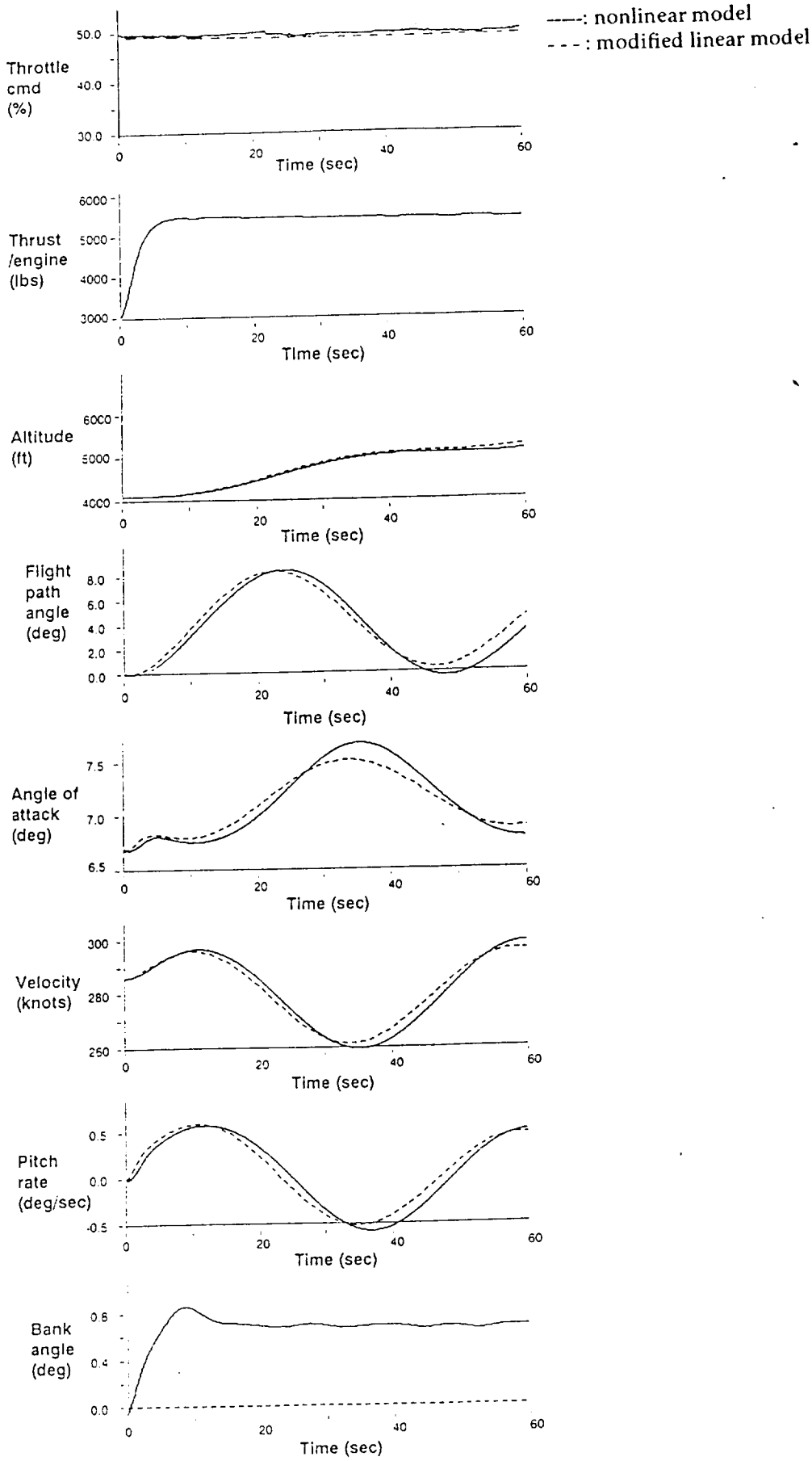

Figure 5. Comparison of the longitudinal open-loop response of the modified B-720 linear model and the nonlinear model, nominal configuration

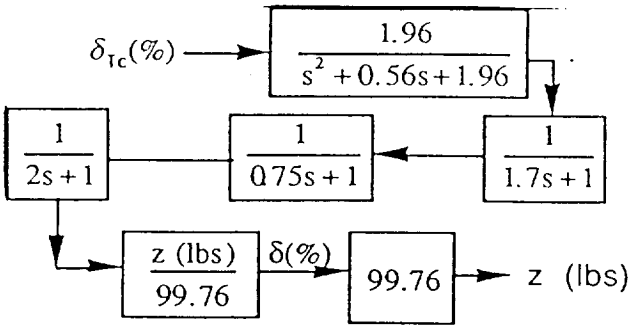

a) Engine spooling block diagrams

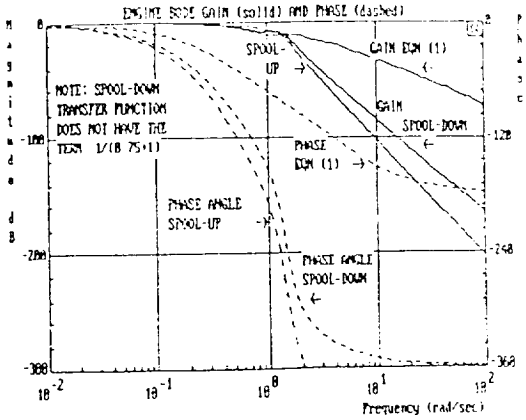

b) Engine δ to δ_{Tc}

Figure 6. Engine spooling block diagrams and Engine δ to δ_{Tc}

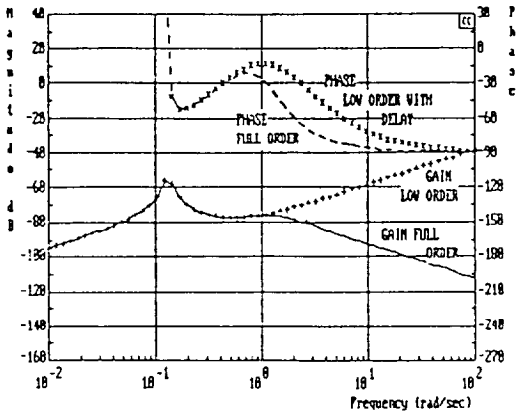

Figure 7. Pitch rate to thrust bode

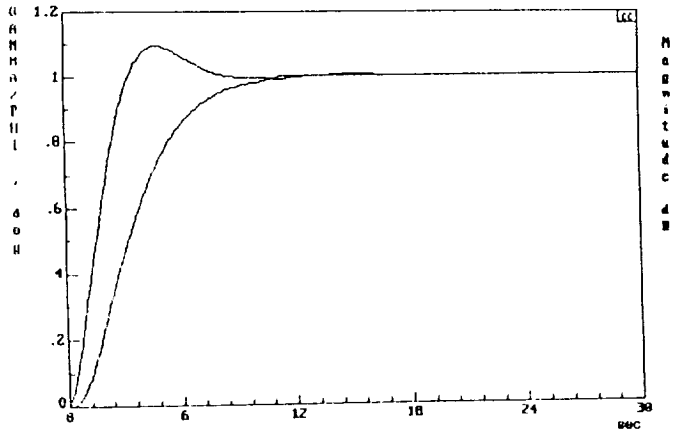

a) Performance specification in time domain

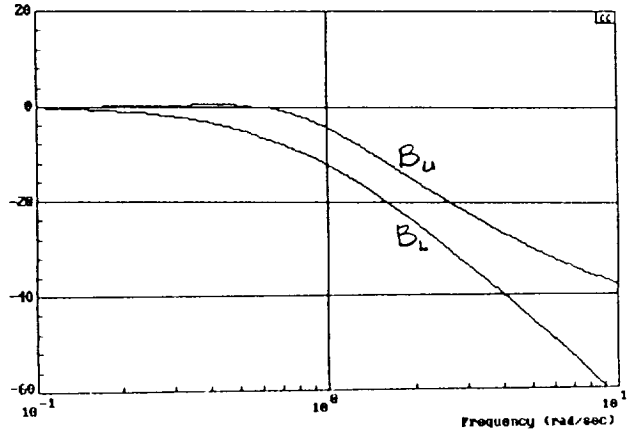

b) Performance specification in frequency domain

Figure 8. Preformance specification in time- and in frequency-domain, for flight path angle and bank angle controls.

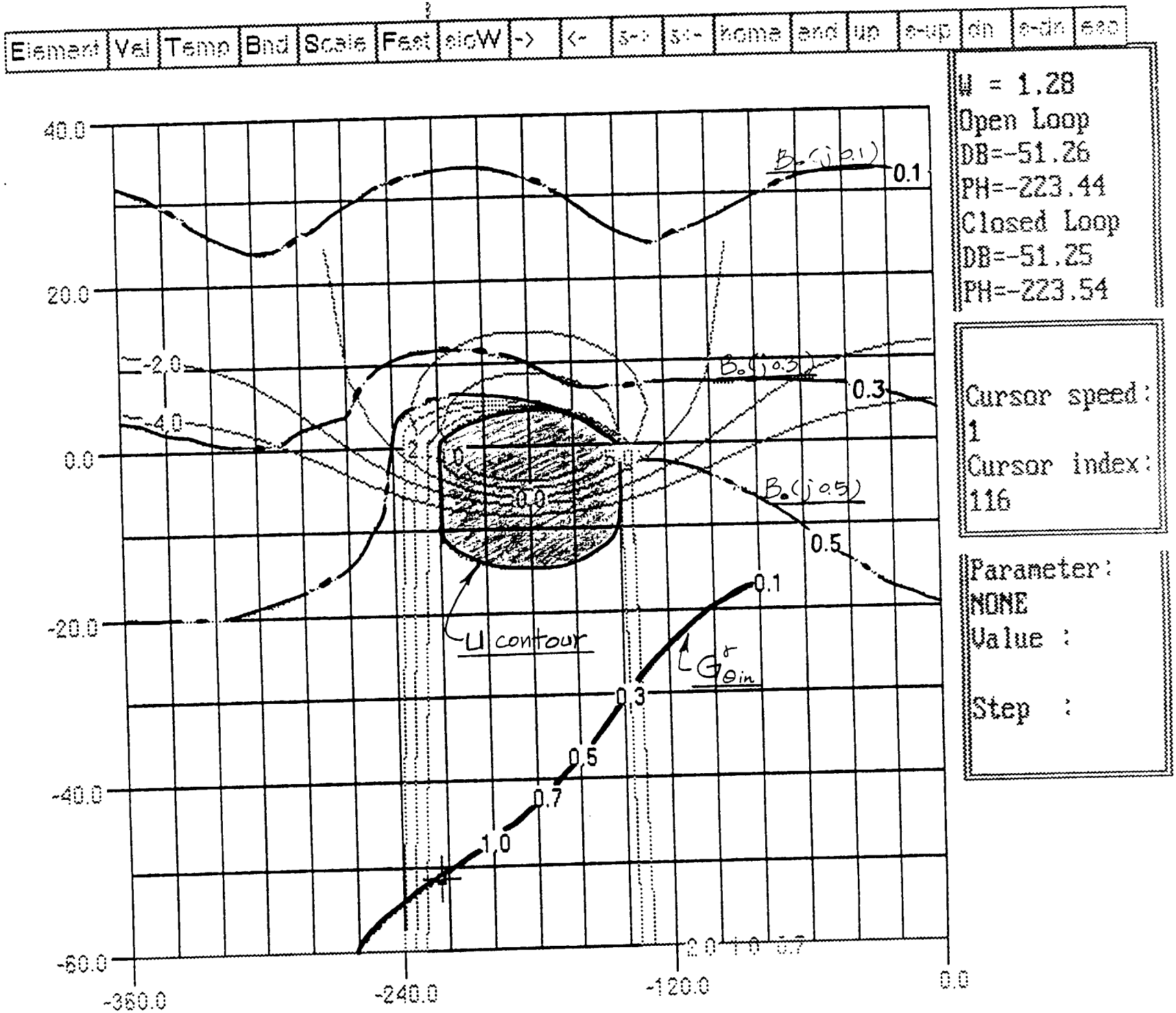

Figure 9. Transfer function $\mathbf{G}^{\gamma}_{\theta_{in}}$, its performance bounds B(jw), and U contour on Nichols Chart

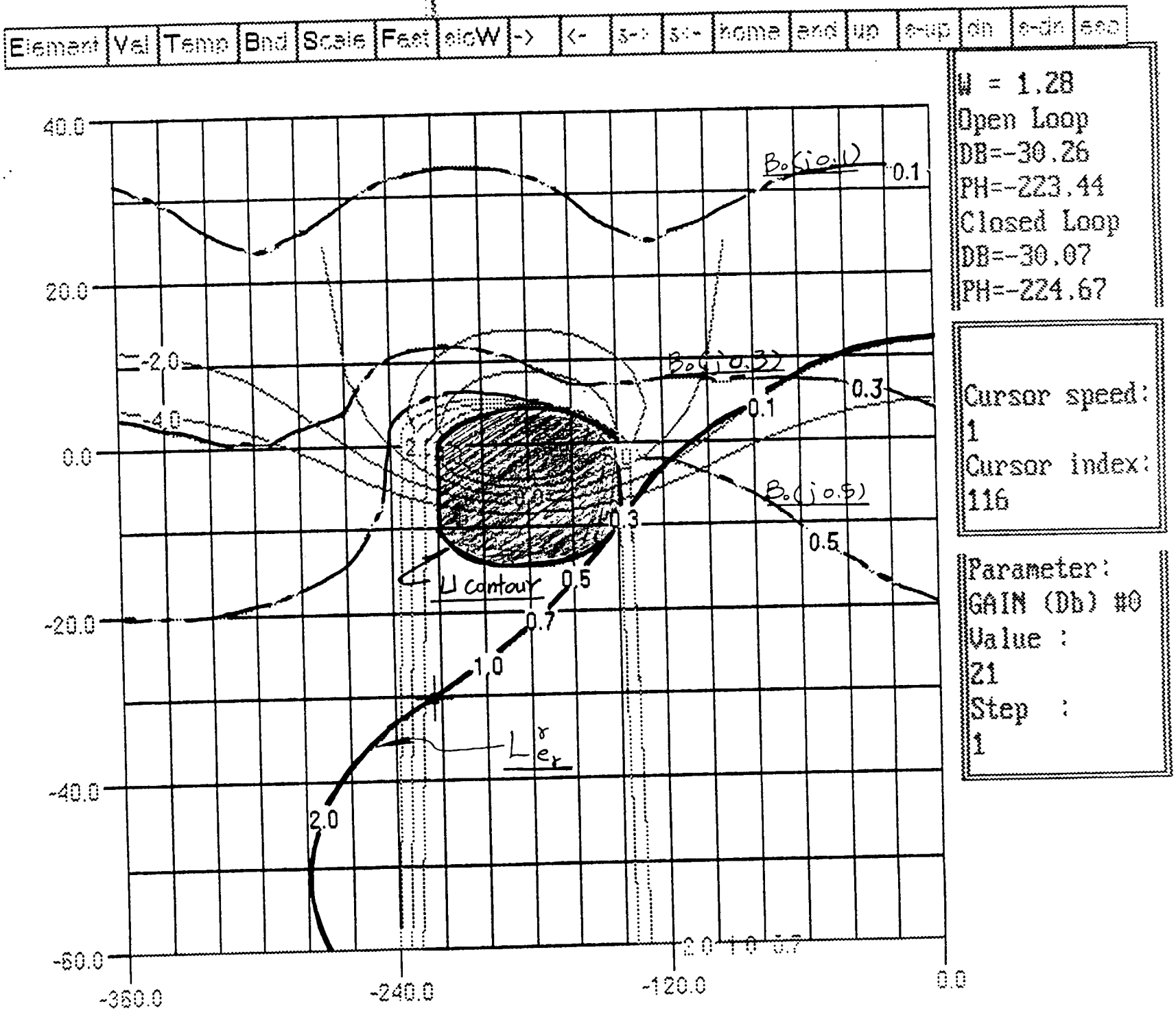

Figure 10. Open-loop transfer function, $\mathbf{L}^{\gamma}_{o_{in}}$, on Nichols Chart

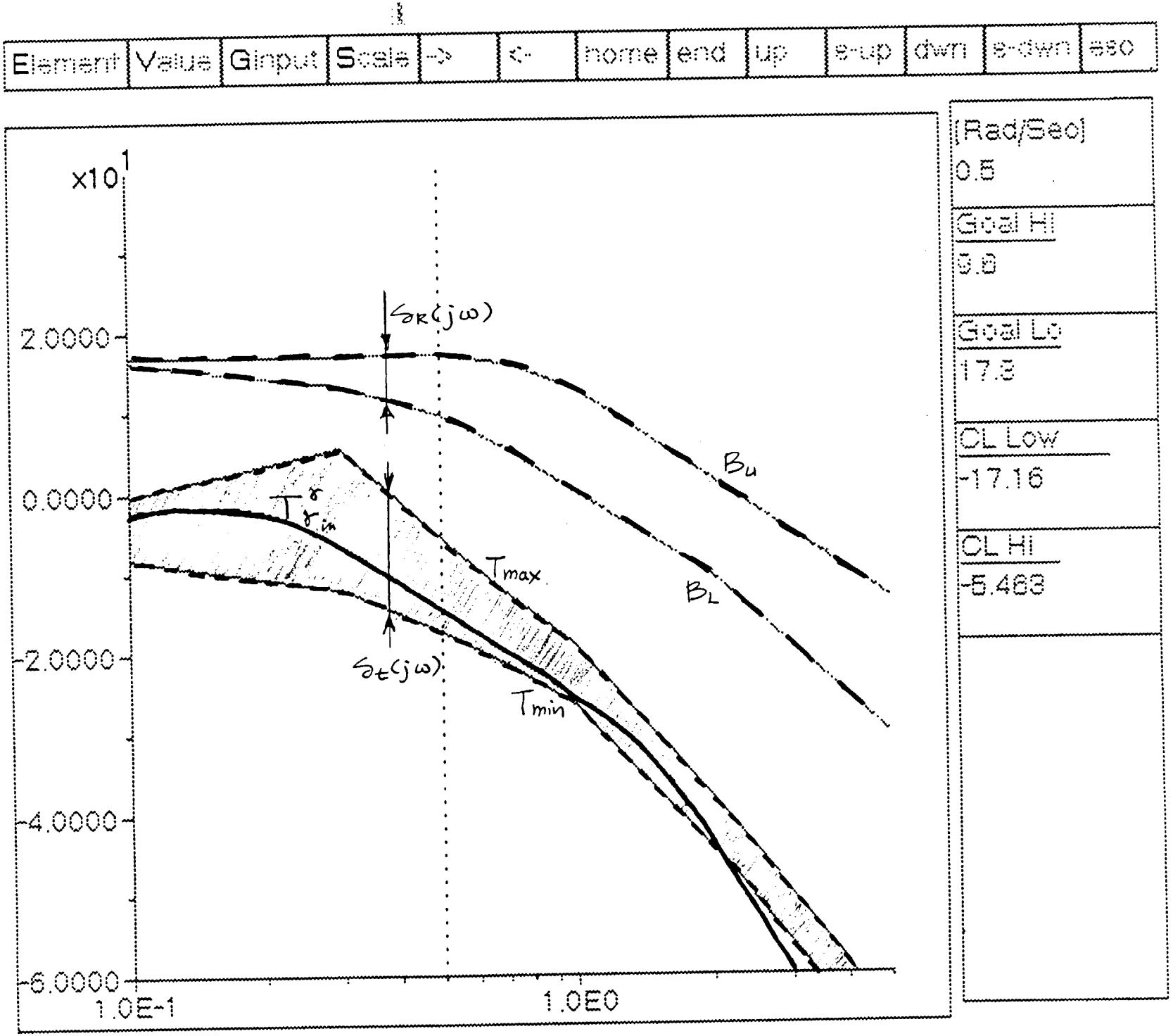

Figure 11. Frequency plot of the close-loop transfer function $\mathbf{T}^{\gamma}_{\gamma_{in}}$ with no prefilter

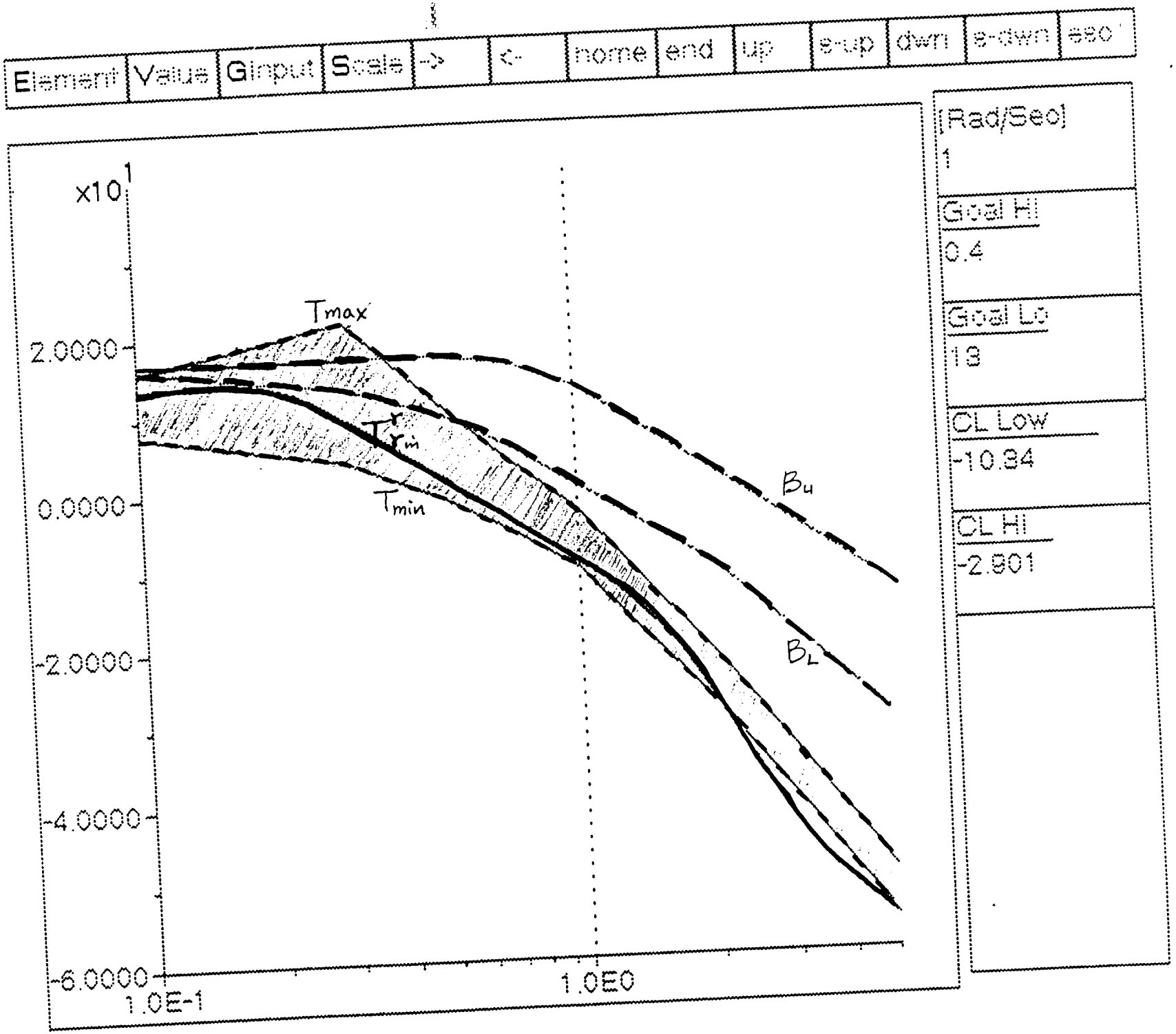

Figure 12. Frequency plot of the close-loop transfer function $\mathbf{T}^{\gamma}_{\gamma_{in}}$ with prefilter

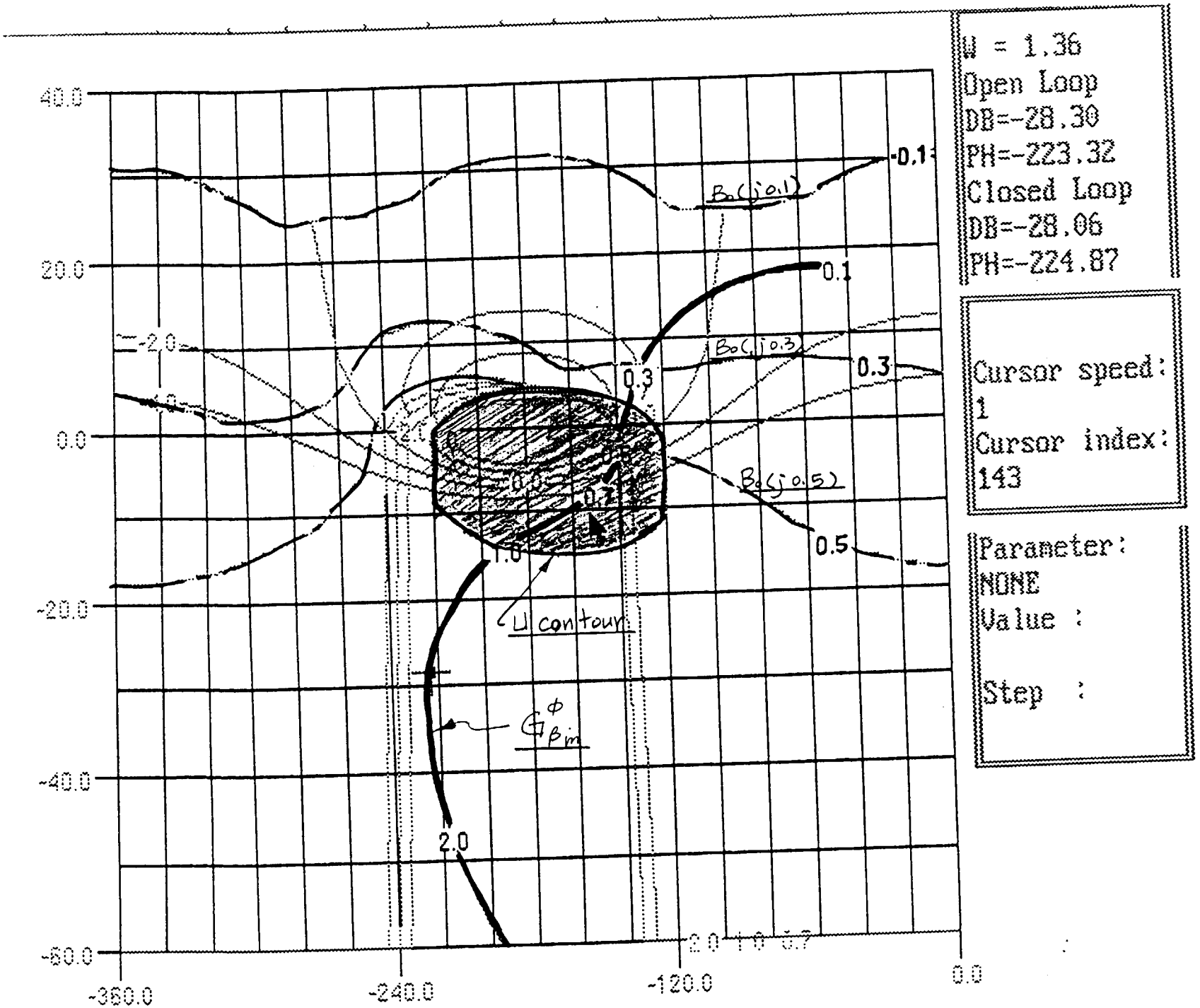

Figure 13. Transfer function $\mathbf{G}^{\phi}_{\beta_{in}}$, its performance bounds B(jw), and U contour on Nichols Chart

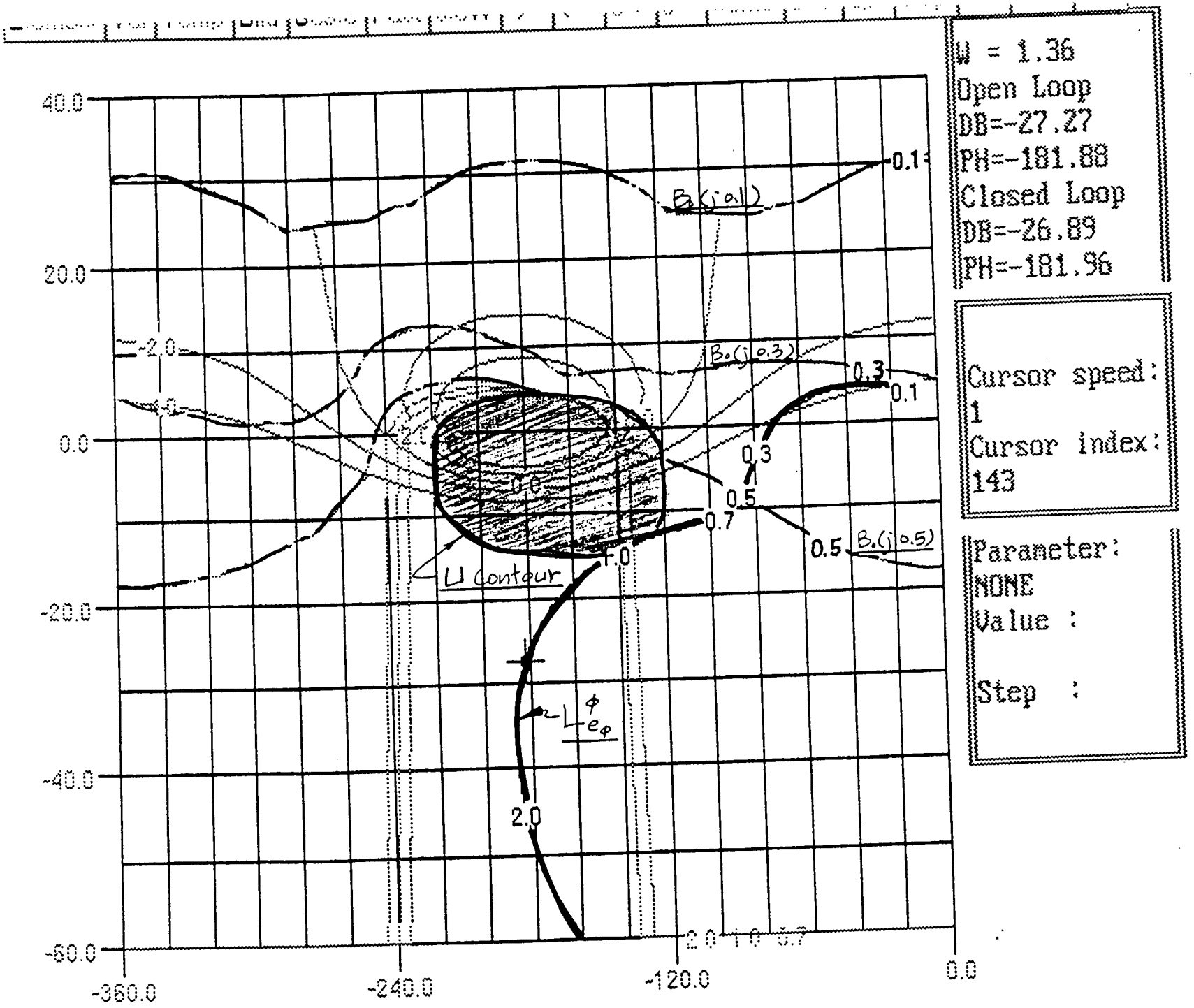

Figure 14. Open-loop transfer function, $\mathbf{L}^{\phi}_{B\phi}$, on Nichols Chart

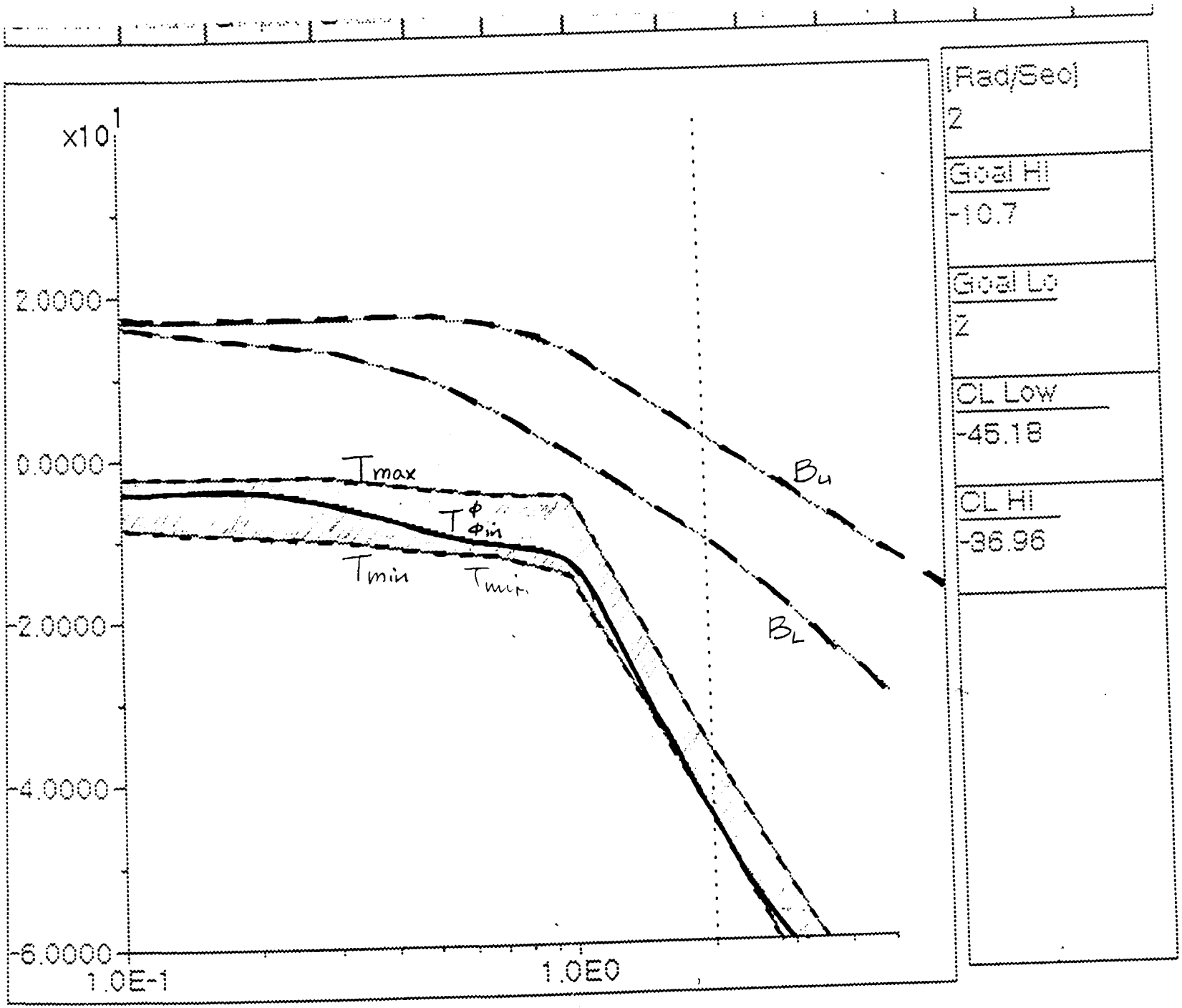

Figure 15. Frequency plot of the close-loop transfer function $\mathbf{T}_{\phi_{in}}^{\phi}$ with no prefilter

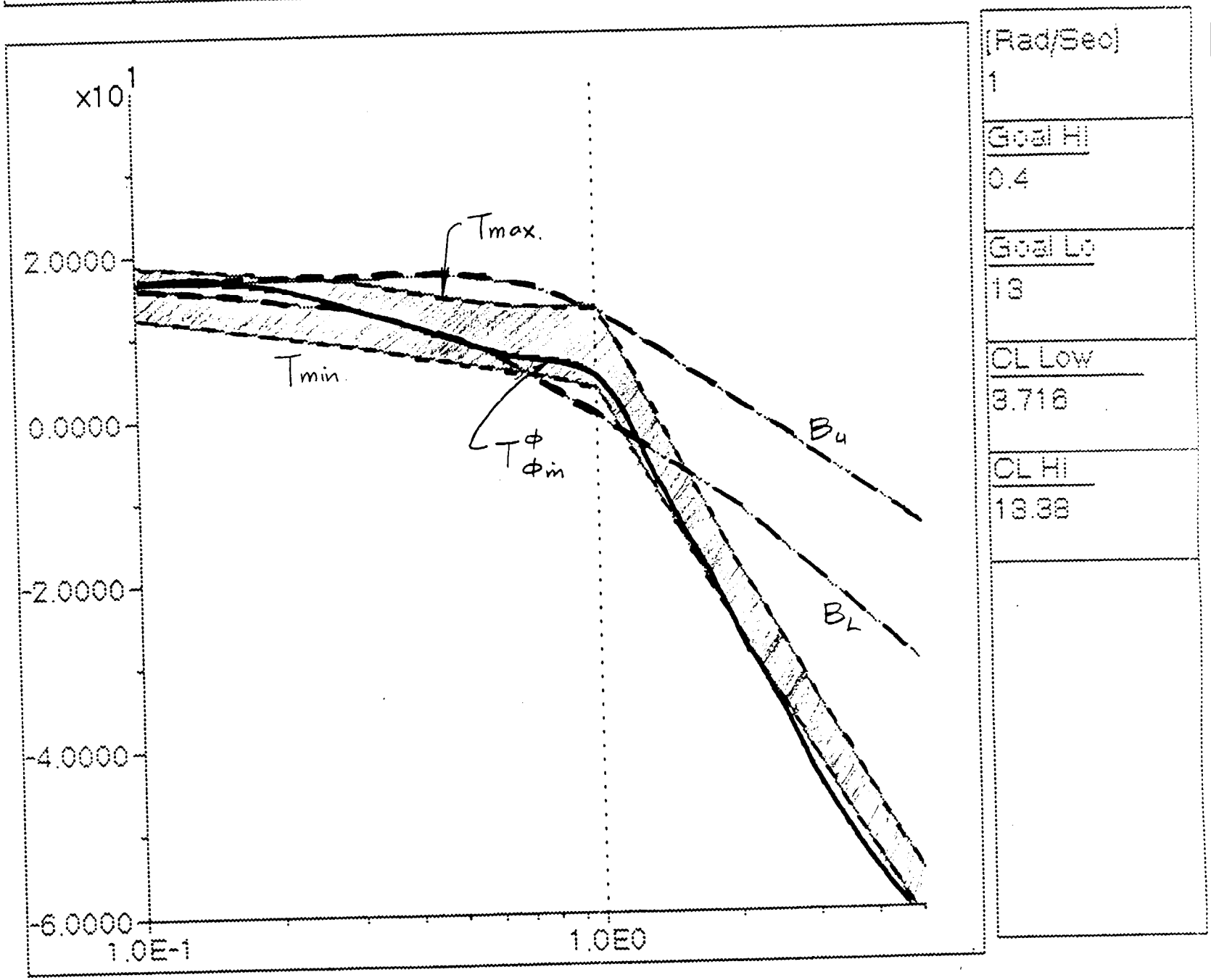

Figure 16. Frequency plot of the close-loop transfer function $\mathbf{T}^{\phi}_{\phi_{in}}$ with prefilter

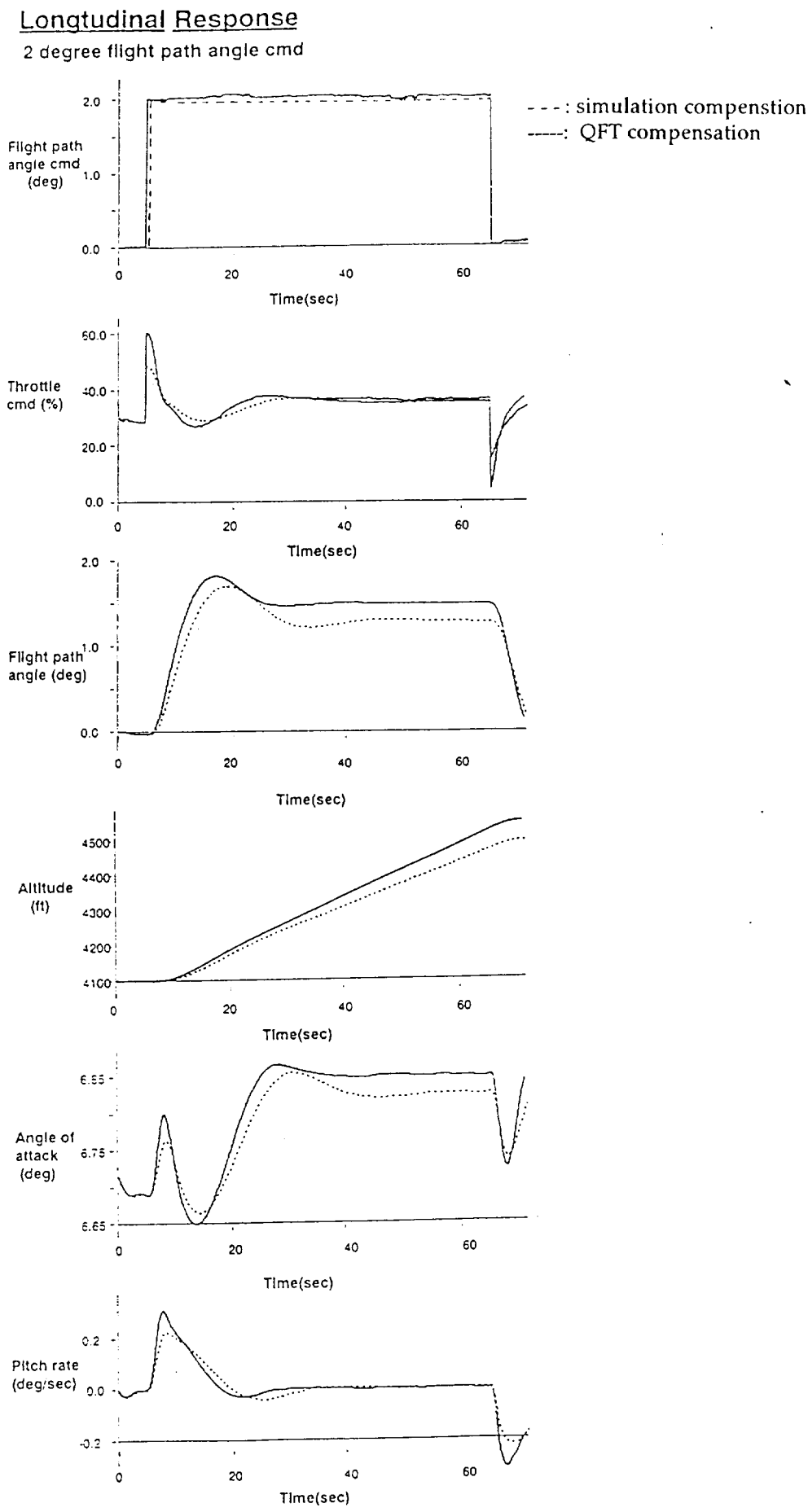

Figure 17. B-720 augmented flight path angle control, step flight path angle response with no turbulence, nominal confiuration

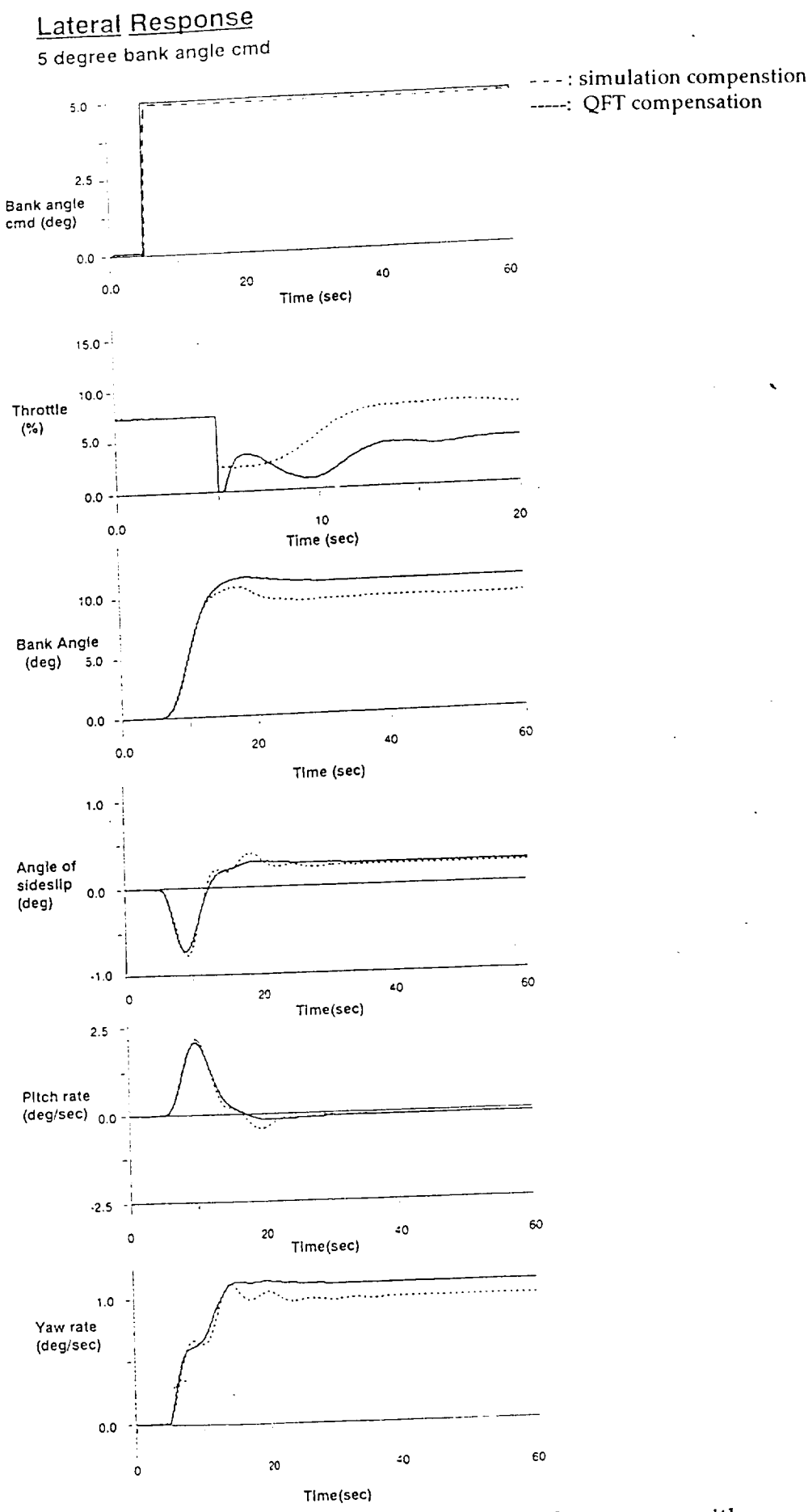

Figure 18. B-720 augmented bank angle control, step bank angle response with no turbulence, nominal confiuration

----- : no turbulence
- - - : intermediate turbulence

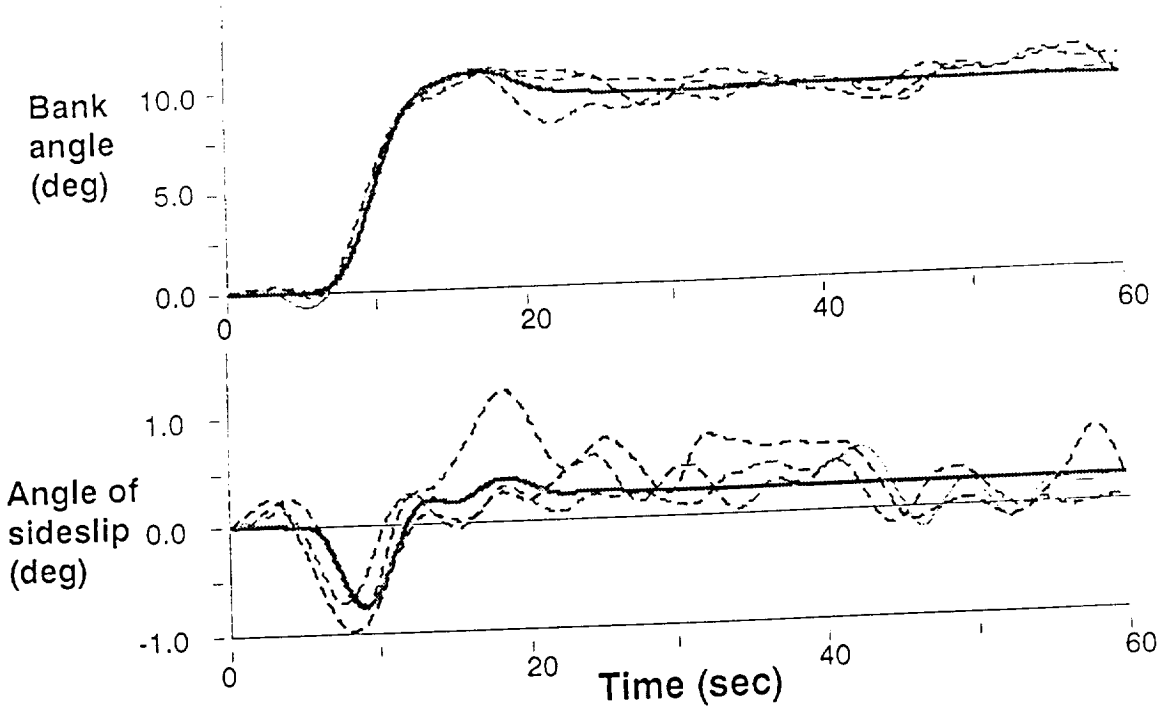

a) Simulation compenstion

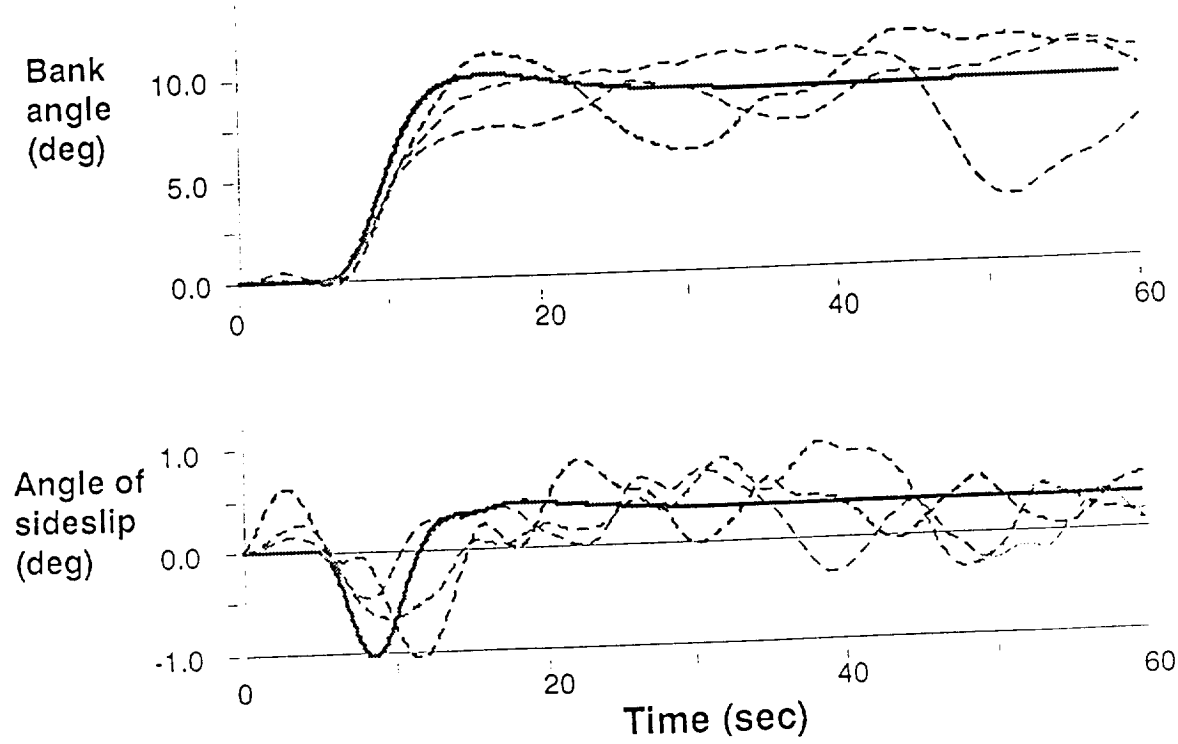

b) QFT compensation

Figure 19. B-720 augmented flight path angle control, step flight path angle response with turbulence, nominal confiuration

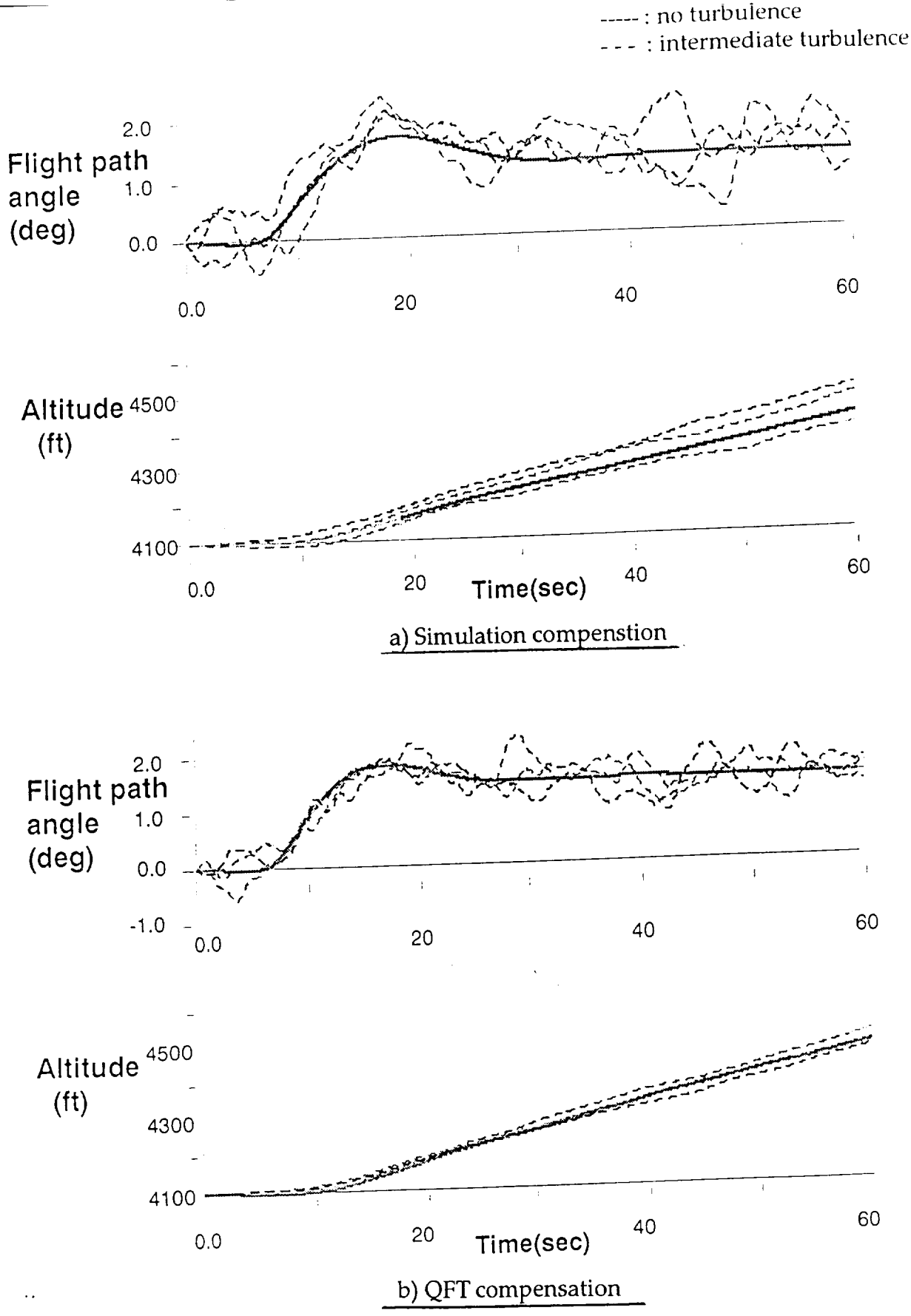

Figure 20. B-720 augmented bank angle control, step bank angle response with turbulence, nominal confiuration

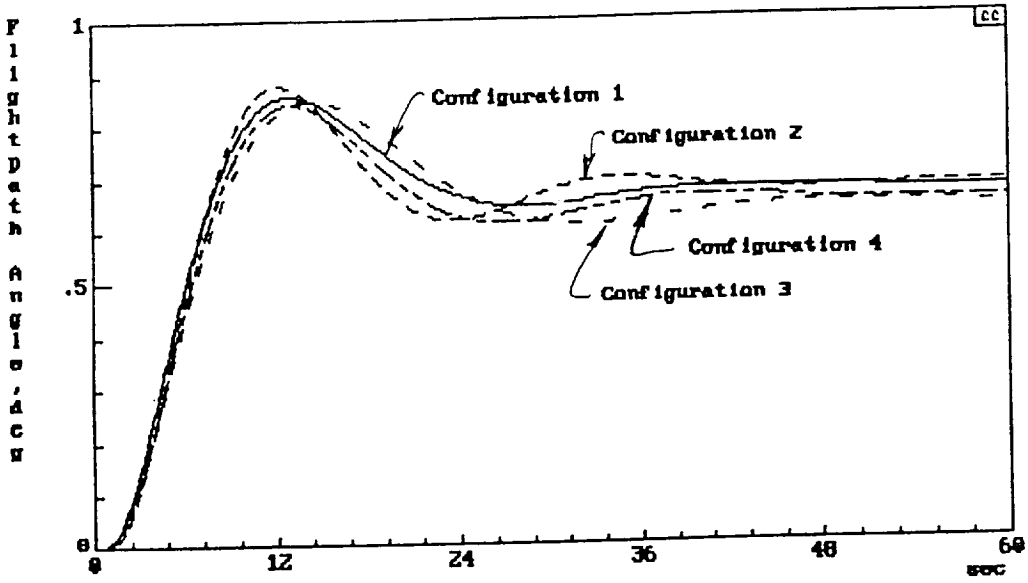

a) Simulation compenstion

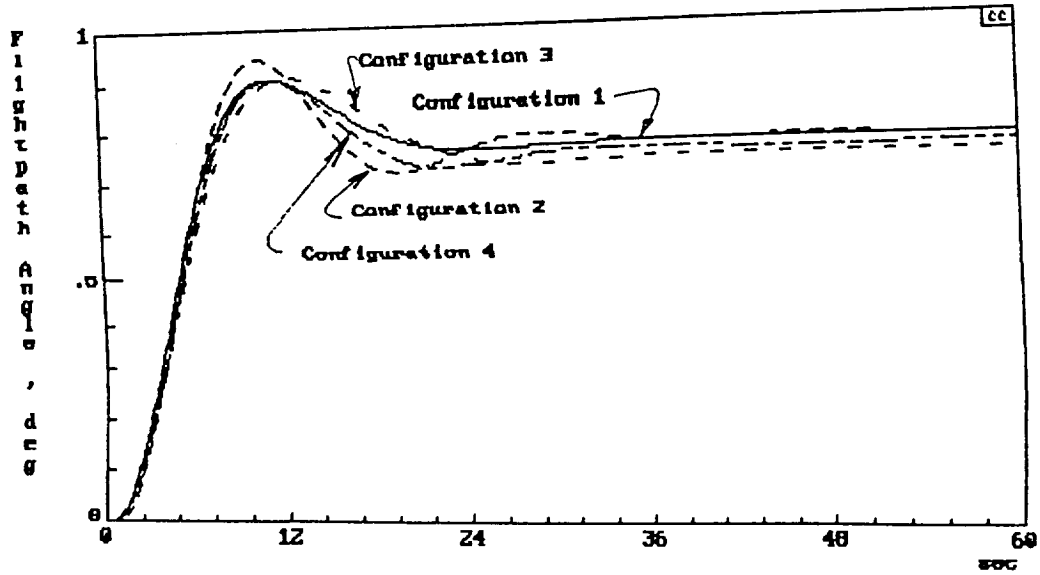

b) QFT compensation

Figure 21. Robustness of the fligh path angle control

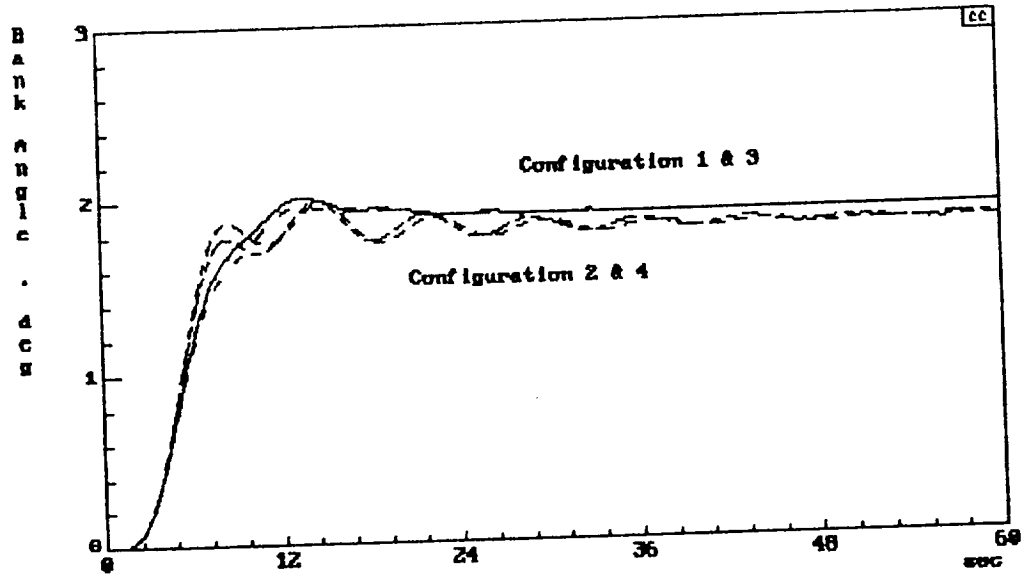

a) Simulation compenstion

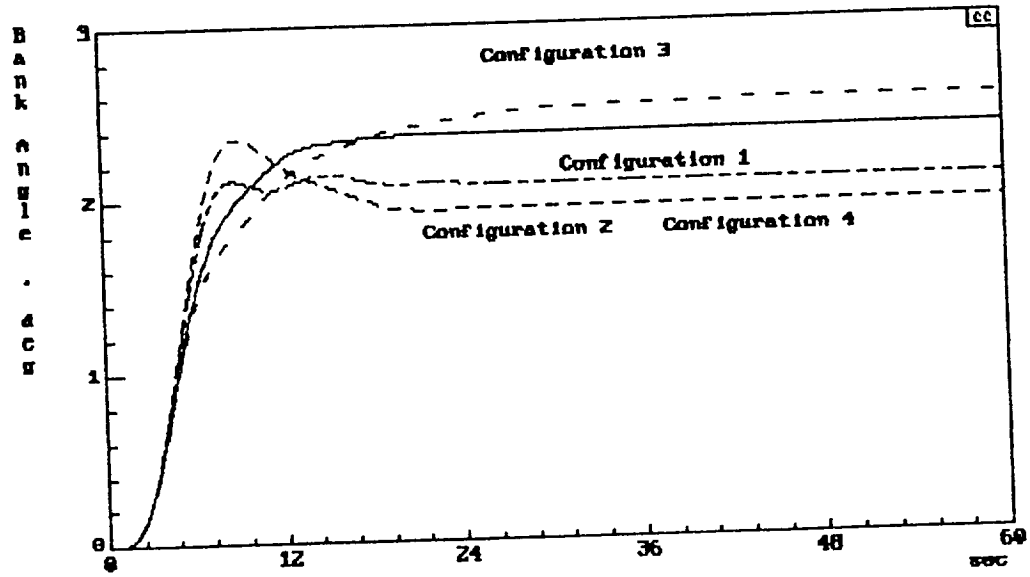

b) QFT compensation

Figure 22. Robustness of the bank angle control

References

1. Burcham, F., Fullerton G., Gilyard, G., Conley, J. and J. Stewart, "A Preliminary Look at Propulsion-Enhanced Flight Controls Research," NASA Dryden document, 1990.

2. Gilyard, G., Conley, J., Le, J., and W. Burcham, "A Simulation Evaluation of a Four-Engine Jet Transport Using Engine Thrust Modulation for Flight Path Control," 27th Joint Propulsion Conference , June 24-26, 1991, Sacramento, CA.

3. Azzano, C.P., "A Preliminary Look at Optimal Multi-Variable Design of Propulsion-Only Flight Controllers for Jet Transport Aircraft," NASA Dryden TR, Sept 21, 1990.

4. Biezad, D.J., "The Propulsive-Only Flight Control Problem," NAECON , Vol 2, pp494-500, Dayton, Ohio, May 20-24, 1991.

5. Biezad, D.J. and C.P. Azzano, "Designing Low Bandwidth Propulsive-Only Flight Controllers", AIAA Guidance, Navigation, and Control Conference, Paper #91-2628CP, pp 267-275, August 12-14, 1991, New Orleans, La.

6. Burcham, F., Fullerton G., Gilyard G., Wolf T., and J. Stewart, "A Preliminary Investigation of the Use of Throttles for Emergency Flight Control," NASA Dryden document, 1991.

7. Thompson, Peter M., Program CC Version 4 Reference Manual: Volume 1, Systems Technology, Inc., November 1988.

8. McRuer, D., Ashkenas, I., and D. Graham, Aircraft Dynamics and Automatic Control, Princeton University Press, 1973.

9. Biezad, D.J., Chou, Hwei-Lan, "Low Bandwidth Robust Controllers for Flight,"NCC2-711, NASA INTERIM REPORT, June-November 1991.

10. J.J., D'Azzo and C.H. Houpis, "Linear control System Analysis and Design Conventional and Modern", McGraw-Hill, 1988.

11. Horowitz,I. M. ,and Sidi,M., "Synthesis of feedback systems with large plant ignorance for prescribed time-domain tolerances" Int. J. Control, Vol.16, pp.287-309, 1972.

12. Horowitz, I.M., Neumann, L., and Yaniv, O., "Quantitative synthesis of uncertain cascaded multiple-input multiple-output feedback systems." Int. J. control, Vol.42, No.2, pp.273-303,1985.

13. Horowitz, I.M., and Yaniv, O., "Quantitative cascaded multiple-input multiple-output synthsis by an improved method." Int. J. Control, Vol.42, pp.305-331, 1985.

14. Horowitz, I.M. and Yaniv, M., "A quantitativedesign method for MIMO linear feedback systems using uncertain plants." Int. J. Control, Vol.43, pp.401-421, 1986.

15. Cole, S., "A computer-aided design package for quantitative feedback theory." M.Sc. Thesis, Air Force Insititude of Technology, 1986.

16. MIL-STD-1797A, "Flying Qualities of Piloted Vehicles", limited distribution, ASD/ENES, Wright-Patterson AFB, Ohio, 30 Jan 1990.

17. Sarrafian, S.K., and Powers, B.G., "Application of Frequency Domain Handling Qualiities Criteria to the Longitudinal Landing Task." NASA Technical Memorandum, Aug. 1985.

18. Gaffney, T., "Pilot in Sioux City jet crash tells story in Dayton," Dayton Daily News, Mar 26, 1991, page 3-A.

19. Leavitt, P., "Crash Settlement," USA Today, Wed, Mar 27, 1991, page 3-A.

20. Roskam, J., Airplane Flight Dynamics and Automatic Flight Controls, Roskam Aviation and Engineering Corp., Ottawa, Kansas, 1979.

21. Blakelock, J., Automatic Control of Aircraft and Missiles, John Wiley & Sons, Inc., 1965.

22. Franklin, G.F., and J. D. Powell, Digital Control of Dynamic Systems, Addison-Wesley, Menlo Park, CA, 1986.

23. J.J., D'Azzo and C.H. Houpis, "Linear control System Analysis and Design

Conventional and Modern", McGraw-Hill, 1988.

24. Wolfe, L.D. and A.E. Fanning, "Advanced Nozzle Technology," AGARD Conference Proceedings CP-241, Fighter Aircraft Design, pp 17-1 to 17-31, Florence, Italy, Oct 1977.

25. Chou, Hwei-Lan, Biezad, D.J., "Pilot-in-the-loop Analysis of Propulsive-only Flight Control Systems", NAECON, Dayton, Ohio, May, 1992

26. Hoh, Roger H. and David G. Mitchell, Flying Qualities of Relaxed Static Stability Aircraft--Volume 1, FAA/CT-82/130-I, Sept, 1982.

APPENDIX A: B-720 CONFIGURATIONS

The B-720 piloted simulation can be represented by the following block diagram:

Flightpath Angle Control Simulation

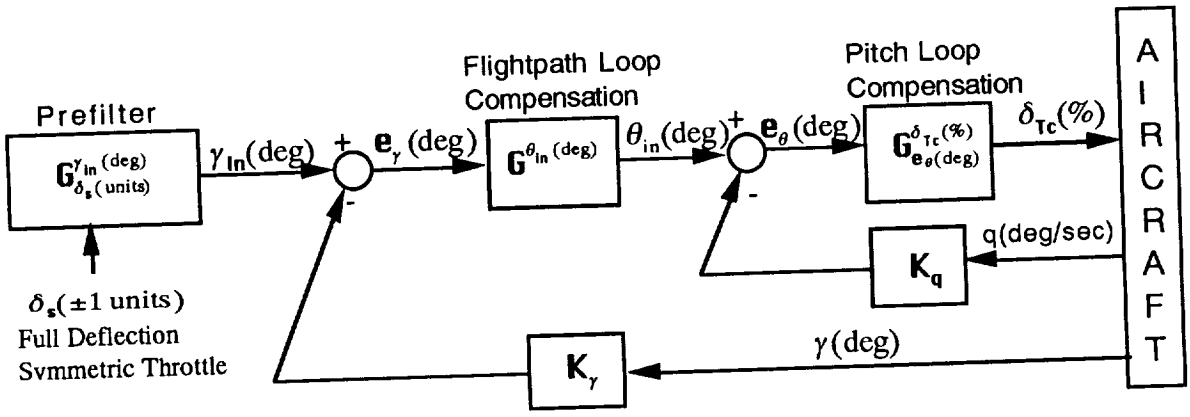

where PF=1, $G_\gamma^{\theta_{in}}$=16, K_γ=1, $G_{e_\theta}^{\delta_{Tc}}$=1, K_q=60

Bank Angle Control Simulation

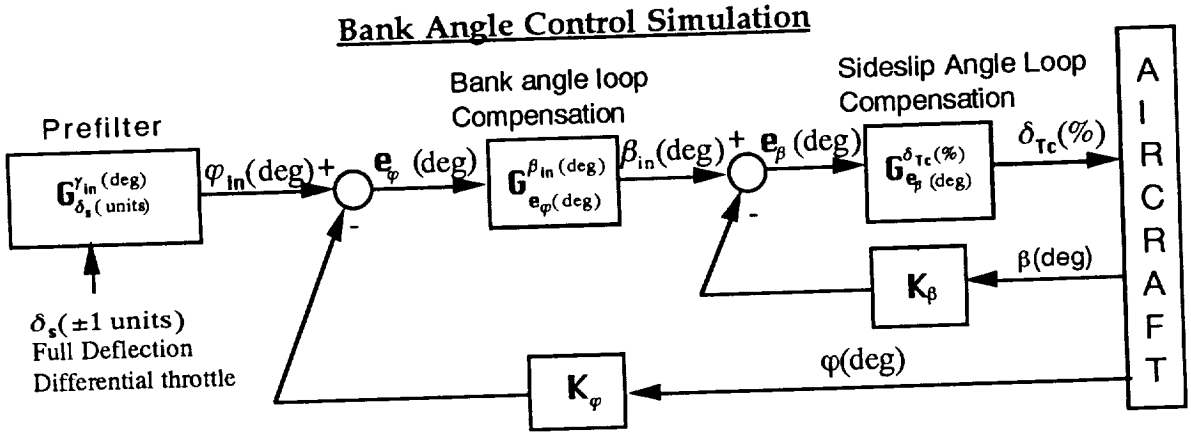

where PF=2.5*(s+.25)/(s+1.25)

$G_\phi^{\beta_{in}}$=1, K_ϕ=(s+.15)/(s+1.5), $G_{e_\beta}^{\delta_{Tc}}$=1, K_β=4

The "AIRCRAFT" in the box above represents both the engine and the bare airframe dynamics. The engine is approximated by a transfer function, G_{eng}, and the bare airframe dynamics are represented mathematically by a single quadruple, $P_{a/c}$, shown as follows.

Longitudinal Dynamics

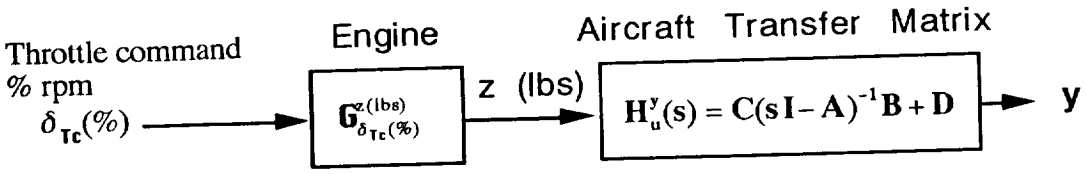

$$\mathbf{P}_{a/c} = \begin{bmatrix} \dot{x} \\ y \end{bmatrix} = \left[\begin{array}{c|c} A & B \\ \hline C & D \end{array}\right] \overset{\text{throttle inputs equal}}{=} \left[\begin{array}{c|c} A & B_1\,(\text{column}) \\ \hline C & D = 0 \end{array}\right]$$

$$\mathbf{x} = [q(\text{deg/sec}) \mid \alpha(\text{deg}) \mid v(\text{kts}) \mid \theta(\text{deg}) \mid h(\text{ft})]'$$

$$\mathbf{y} = [n_{\text{pilot gs}} \mid n_{\text{fcs g's}} \mid q \mid \alpha \mid v \mid \theta \mid h \mid \gamma(\text{deg})]'$$

$$\mathbf{u} = [z_{\text{outbd left}}(\text{lbs}) \mid z_{\text{inbd left}}(\text{lbs}) \mid z_{\text{inbd right}}(\text{lbs}) \mid z_{\text{outbd right}}(\text{lbs})]'$$

$\mathbf{u}_1 = z(\text{lbs})$ [used when all throttles have same command]

Lateral Dynamics

$$\begin{bmatrix} \dot{x} \\ y \end{bmatrix} = \left[\begin{array}{c|c} A & B \\ \hline C & D \end{array}\right] \begin{bmatrix} x \\ u \end{bmatrix} = \left[\begin{array}{c|c} A & B_2 \\ \hline C & D = 0 \end{array}\right] \begin{bmatrix} x \\ u_2 \end{bmatrix}$$

where

$$\mathbf{P}_{a/c} = \left[\begin{array}{c|c} A & B \\ \hline C & D \end{array}\right] \quad \text{.....for four engine inputs, u}$$

$$= \left[\begin{array}{c|c} A & B_2 \\ \hline C & D = 0 \end{array}\right] \quad \text{.....for one total engine input, } u_2$$

$$\mathbf{x} = [p(\text{deg/sec}) \mid r(\text{deg/sec}) \mid \beta(\text{deg}) \mid \phi(\text{deg})]'$$

$$\mathbf{y} = \left[A_{Y_{c.g.}} \mid p(\text{deg/sec}) \mid r(\text{deg/sec}) \mid \beta(\text{deg}) \mid \phi(\text{deg})\right]'$$

$$\mathbf{u} = [z_{\text{outbd left}}(\text{lbs}) \mid z_{\text{inbd left}}(\text{lbs}) \mid z_{\text{inbd right}}(\text{lbs}) \mid z_{\text{outbd right}}(\text{lbs})]'$$

$\mathbf{u}_2 = [z(\text{lbs})]$, where $z = z_{\text{outbd left}} + z_{\text{inbd left}} + (-z_{\text{inbd right}}) + (-z_{\text{outbd right}})$

The B metrix has four columns, each column is to be multiplied by the thrust input from each engine that given in matrix u. If symmetric throttle is given(assume all four throttles are given the same command), the **B** matrix in longitudinal dynamics becomes a single column. Each row value in this column matrix $\mathbf{B_1}$ is equal to the sum of the corresponding row elements in the full order **B** matrix representing four engines. If differential throttle is given(i.e. the left engines and right engines are given same amount of command but in opposite direction), the **B** matrix in lateral dynamics becomes another single column matrix, $\mathbf{B_2}$. Each row element in $\mathbf{B_2}$ is the sum of

the positive value of column 1 & 2 and negative value of column 3 & 4 of each row in **B**. The open-loop configuration then becomes **P=Pa/c*Peng**, where **Peng** is the quadruple form of the engine transfer function, $G^{z(lbs)}_{\delta_e(\%)}$. The quadruples for four different configurations were obtained as described in Reference.

The flight conditions for each configurations are summarized in the table below.

Configuration Summary

Config. Number	Weight (lbs)	Altitude (Ft MSL)	Airspeed (Knots)	Flaps (%)	Gear up/down
1	140,000	4,000	160	0	up
2	140,000	4,000	145	30	up
3	160,000	4,000	175	0	up
4	140,000	4,000	155	30	up

The transfer functions were obtained from the quadruples using System Technology's CC Program. These aircraft transfer functions are listed here with each respective row of numbers designating the corresponding configuration transfer function values. The nominal configuration, number 1, is represented by values in each row 1 below.

Longitudinal Transfer Functions

$$N^{q(deg/sec)}_{z(lbs)} = N^{q(deg/sec)}_{z(lbs)} / \Delta_{long}$$

$$N^{\gamma(deg)}_{z(lbs)} = N^{\gamma(deg)}_{z(lbs)} / \Delta_{long}$$

$$N^{q(deg/sec)}_{z(lbs)} = \begin{array}{|l|l|l|l|} \hline 2.36E-04 & (0) & (-1.17E-05) & (0.40) \quad (0.61) \\ \hline 2.33E-04 & (0) & (1.4E-06) & (0.635 , \ 0.563) \\ \hline 1.976E-04 & (0) & (0.292) & (0.644) \\ \hline 1.955E-04 & (0) & (2.68E-06) & (0.819 , \ 0.508) \\ \hline \end{array}$$

$$N^{\gamma(deg)}_{z(lbs)} = \begin{array}{|l|l|l|l|} \hline 2.796E-05 & (0) & (0.203) & (0.370 , \ 3.008) \\ \hline -1.819E-05 & (0) & (0.364) & (2.255) \quad (-4.452) \\ \hline 2.130E-05 & (0.167) & (0.351 , & 3.038) \\ \hline 1.470E-05 & (0) & (0.261) & (0.460 , 3.426) \\ \hline \end{array}$$

$$\Delta_{long} = \begin{array}{|l|l|l|} \hline (1.438E-05) & (3.918E-02\ ,\ 0.130) & (0.652\ ,\ 1.382) \\ \hline (1.101E-05) & (7.423E-02\ ,\ 0.147) & (0.596\ ,\ 1.375) \\ \hline (3.949E-02\ ,\ 0.118) & (0.649\ ,\ 1.301) & \\ \hline (1.878E-05) & (7.190E-02\ ,\ 0.138) & (0.588\ ,\ 1.279) \\ \hline \end{array}$$

Lateral Transfer Functions

$$N_{Z(lbs)}^{\beta(deg)} = N_{Z(lbs)}^{\beta(deg)} / \Delta_{lat}, \qquad N_{Z(lbs)}^{\beta(deg)} = \begin{array}{|l|l|l|} \hline -1.58E-03 & (-.0805) & (.927) \\ \hline -1.59E-03 & (-.0922) & (.904) \\ \hline -1.43E-03 & (-.0723) & (.981) \\ \hline -1.44E-03 & (-.0879) & (.940) \\ \hline \end{array}$$

$$N_{Z(lbs)}^{\phi(deg)} = N_{Z(lbs)}^{\phi(deg)} / \Delta_{lat}, \qquad N_{Z(lbs)}^{\phi(deg)} = \begin{array}{|l|l|} \hline 3.19E-04 & (.468\ ,\ 3.65) \\ \hline 2.15E-04 & (.611\ ,\ 4.17) \\ \hline 2.89E-04 & (.447\ ,\ 3.96) \\ \hline 2.04E-04 & (.593\ ,\ 4.33) \\ \hline \end{array}$$

$$\Delta_{lat} = \begin{array}{|l|l|l|} \hline (.0001) & (1.01) & (.116\ ,\ 1.05) \\ \hline (.006) & (1.05) & (.067\ ,\ 0.93) \\ \hline (.0028) & (1.06) & (.114\ ,\ 1.08) \\ \hline (.0065) & (1.09) & (.060\ ,\ .944) \\ \hline \end{array}$$

The engine transfer function for all configurations is given in short form notation by

$$G_{\delta_{tc}(\%)}^{Z(lbs)} = \frac{275}{(0.55)(5)}$$

Configuration Storage Table for Quadruples

*Pxxxx.4U : Quadruple with four engine inputs

*Pxxxx.1U : Quadruple with one total engine input

Dynamics	Config. Number	Quadruple $P_{a/c}$	Quadruple $P_{a/c}$*P_{eng}
Longitudinal	1 1	P1000.4U P1000.1U	- P100
Longitudinal	2 2	P2000.4U P2000.1U	- P200
Longitudinal	3 3	P3000.4U P3000.1U	- P300
Longitudinal	4 4	P4000.4U P4000.1U	- P400
Lateral	1 1	P5000.4U P5000.1U	- P500
Lateral	2 2	P6000.4U P6000.1U	- P600
Lateral	3 3	P7000.4U P7000.1U	- P700
Lateral	4 4	P8000.4U P8000.1U	- P800

Appendix B: Overview of QFT Design Method

Quantitative Feedback Theory(QFT) is a theory that emphasizes the use of feedbacks to achieve a desired system performance while incorporating plant uncertainty and plant disturbance into control design [17-23]. The QFT technique provides several advantages:

- QFT technique provides good insight throughout the process of controller design.
- QFT technique allows the designer to specify a desired close-loop performance.
- QFT technique allows the designer to incorporate plant uncertainty and plant disturbance into controller design.
- QFT technique will design a robust controller that meets the prescribed performance specification over the full range of plant uncertainty.

The basic design procedures of the QFT technique for minimum phase systems are:

1) Model the system into a unit feedback SISO/MISO system to apply QFT. A m x m MIMO system can be converted into m-equivalent SISO/MISO systems and the coupling between loops can be considered as disturbance input. Fig. B-1 shows a general SISO/MISO system for QFT application.

2) Specify a desired close-loop frequency response. Fig. B-2 shows the construction of a desired close-loop performance, with an upper bounds, B_u, a lower bound, B_L, and a tolerance, δ_R, and also a maximum allowable close-loop magnitude, M_m. The upper bound is generally described by an underdamped closed loop response and the lower bound an overdamped closed loop response. Fig. B-3 shows the construction of a desired disturbance performance specification which only has a upper bound. The objective is to design a controller such that the variation of the response due to plant uncertainty lies within the specified boundaries and the effect of disturbance is minimized, that is to have:

$$B_L(\omega) \le |T_R(j\omega)| \le B_U(\omega)$$

$$|T_{D1}(j\omega)| \le |M_D(j\omega)|$$

$$|T_{D2}(j\omega)| \le |M_D(j\omega)|$$

3) Convert the performance tolerance, δ_R, and the maximum M_m onto Nichols Chart to form design constraints: performance bounds,$B(j\omega_i)$, and the U contour.

   i) Performance bounds are constraints to ensure that at each frequency, the variation of the system response, δ_T, due to plant uncertainty does not exceed the prescribed performance tolerance, δ_R.

ii) The U contour is a constraint to ensure the system damping will be kept no less than the damping correlates to the maximum M_m. Figure 4 shows the construction of a U contour.

4) Reshape the plant transfer function. With the plant transfer function, P_o, and the design constraints: performance bounds, $B(j\omega_i)$, and the U contour, all displayed on Nichols Chart, reshaping may be done by adding poles/zeros/gain compensation to P_o to reshape P_o to satisfy those constraints. After reshaping, P_o becomes L_o, and the poles/zeros/gain added to compensate P_o forms the controller, G_c, as can be depicted from this relationship:

$$L_o = P_o * G_c$$

To satisfy those constraints, each frequency ω_i on L_o should be kept on and above it corresponding $B(j\omega_i)$; L_o should also not penetrate the U contour. Figure B-5 shows the U contour, performance bounds and the optimal L_o of an example problem.

5) After reshaping(compensation), the system is guaranteed robust over the full range of plant uncertainty, i.e. $\delta_T(jw_i) \leq \delta_R(jw_i)$. However, the system may not have met the performance specifications completely yet(see Figure B-6.) A prefilter may be required to reposition the compensated system to fully meet the specification.

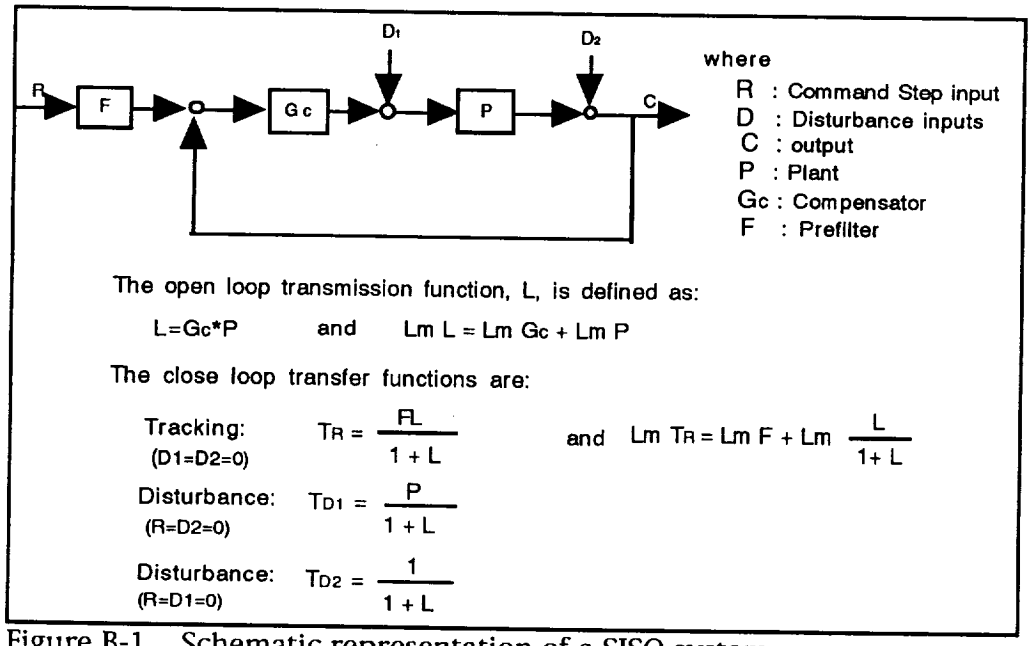

Figure B-1. Schematic representation of a SISO system

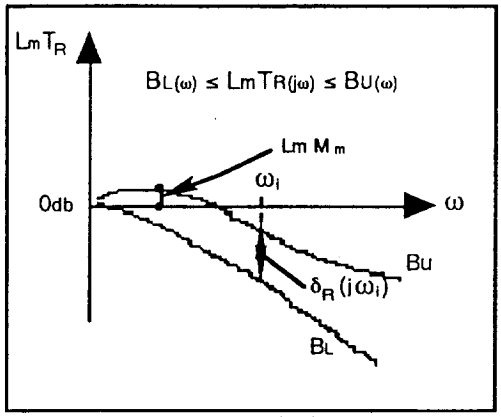

Figure B-2. Typical closed loop tracking specification

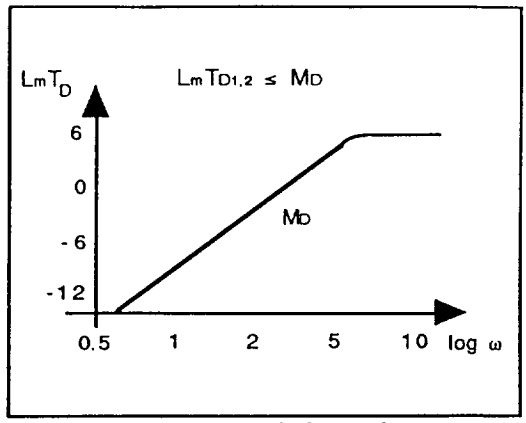

Figure B-3. Typical disturbance rejection specification

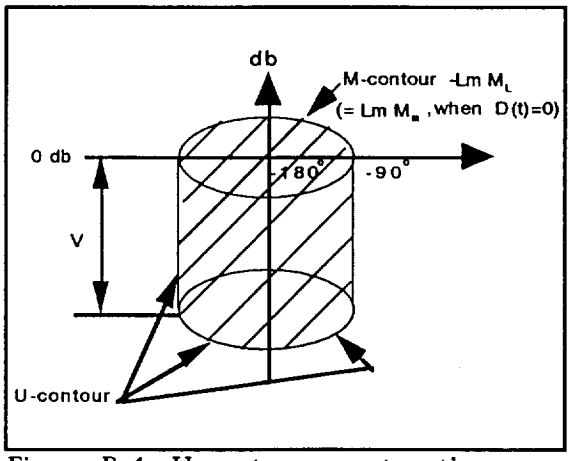

Figure B-4. U contour construction

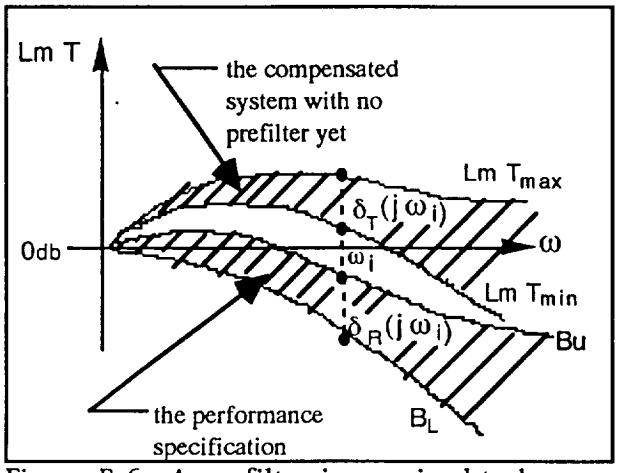

Figure B-6. A prefilter is required to have the compensated system to fully meet the performance specification

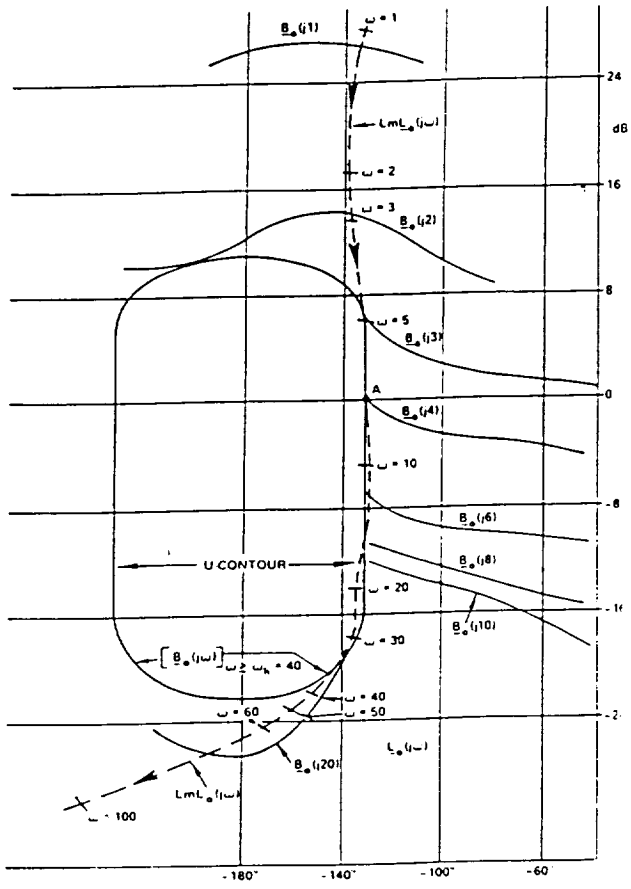

Figure 5. Reshaping the plant transfer function